The Organic-Mineral Interface in Biominerals

P. U. P. A. Gilbert*, Mike Abrecht, Bradley H. Frazer

University of Wisconsin-Madison
Department of Physics, and Synchrotron Radiation Center
3731 Schneider Drive
Stoughton, Wisconsin, 53589, U.S.A.
pupa@src.wisc.edu
*previously publishing as Gelsomina De Stasio

BIOMINERALS: TOUGH STRUCTURES OF LIFE

Introduction to biominerals

Numerous living organisms form minerals. These biogenic minerals, or biominerals, are composite materials containing an organic matrix and nano- or micro-scale amorphous or crystalline minerals. In this chapter we will review the molecular aspects of biomineralization and describe as completely as is currently possible the organic-mineral interface, the location in which organic-mineral interactions occur. Biomineral composite materials include bone, dentine, enamel, statoliths, otoliths, mollusk and crustacean shells, coccolith scales, eggshells, sponge silica skeletons, algal, radiolarian and diatom silica micro-shells, and a variety of transition metal minerals produced by different bacteria (Lowenstam and Weiner 1989; Addadi and Weiner 1997; Banfield and Nealson 1997; Fortin et al. 1997; Fitts et al. 1999; Templeton et al. 1999; Lower et al. 2001a; Mann 2001; Glasauer et al. 2002; De Yoreo and Vekilov 2003; Weiner and Dove 2003; De Yoreo and Dove 2004).

From a materials science perspective, organic molecules are soft, compliant and fracture resistant while inorganic crystals are hard and brittle. Biomineral composites combine the best of these properties and minimize the weaknesses: they are both hard and fracture resistant (tough) (Currey 1977; Jackson et al. 1988; Schäffer et al. 1997; Kamat et al. 2000; Gao et al 2003). This is due to several factors: structure, nano-size and chemical composition. Only recently materials scientists have begun to learn how to build a synthetic composite material that outperforms each component taken separately, and have done so inspired by shell nacre (Tang et al. 2003).

The mechanisms of biomineral formation are not fully understood (Mount et al. 2004) and while they are of interest in their own right, they may also provide models for new materials concepts, inspire design solutions and give new insights into the genetic control of biological structure (e.g., Schäffer et al. 1997).

Lowenstam (1981) introduced the distinction between the biologically induced mineralization, which is enacted extracellularly or on the cell surface by many algae and bacterial species, and the organic-matrix mediated mineralization performed by many animals (later termed biologically controlled mineralization) (Bazylinski and Frankel 2003; Frankel and Bazylinski 2003; Veis 2003).

Eukaryotic biominerals often show complex hierarchical structure from the nanometer to the macroscopic scale. This structure confers mechanical strength and toughness: despite being highly mineralized, with the organic component constituting not more than a few percent of the composite material, the fracture toughness exceeds that of single crystals of the

pure mineral by two to three orders of magnitude (Kamat et al. 2000). The recent discovery of the silica skeleton in *Euplectella* sp., and its seven levels of structural organization illustrates one brilliant such hierarchy (Aizenberg at al. 2005), as reported in Figures 1 and 2.

In eukaryotes biominerals provide a variety of functions including mechanical protection, movement, grinding, gravity or magnetic field sensing. Conversely in prokaryotes biominerals are often formed as a byproduct of a biochemical pathway in which the bacteria oxidize or reduce transition metals or other species in solution, often for metabolic energy generation (Nealson and Stahl 1997; Frankel and Bazylinski 2003).

Why biominerals

For prokaryotes and eukaryotes the complex bioinorganic chemistry involved in biomineralization constitutes a distinct evolutionary advantage for the organism performing it. That advantage is the reason biomineralization became as widely spread as is observed in the three kingdoms of life: Archaea, Bacteria, and Eukarya (protists, fungi, plants, and animals), although very few Archaea are known to be biomineral producers. In the cases of eukaryotic biominerals, the biomineral products are clearly of direct use and benefit. In the case of microbial biomineralization, metal oxidation or reduction can be induced - or exploited - by the bacterium, but mineralization itself may have only indirect advantages or even disadvantages. Biomineral formation often occurs extracellularly and is subsequent to oxidation or reduction. In some cases it is detrimental: entombment of the bacterium in its own biomineral products is possible, and the cell either dies or develops an evasion strategy, such as the formation of mineral sheaths (e.g., *Leptothrix spp*) or stalks (*Gallionella ferruginea*).

The organic-mineral interface

Many biomineralization mechanisms are poorly understood at the molecular level. These include all cases in which highly oriented crystals are formed with the growth of a particular crystal phase, or polymorph (Falini et al. 1996; De Yoreo and Dove 2004). Mollusk shell, bone and some bacterial filaments are examples of such biomineralization: a highly specialized organic matrix directs the formation of a specific crystal phase, habit, size and orientation. In these composites the organic-mineral interaction is so specialized that a mechanism of epitaxial overgrowth, or templation, can be invoked. The particular matrix of organic molecules, produced by the living organism, acts as a template upon which crystals grow epitaxially, or simply, growth is nucleated, and crystal structure, phase, orientation and often habit of the mineral are determined by the organic matrix. Figure 3 shows a biomineralization paradigm.

The paradigm of Figure 3 is not general: it applies to some prokaryotic and many eukaryotic biominerals. It is simply intended to guide our reasoning and give a visual model to refer to in this discussion; it is by no means intended to describe and include every biomineral formation mechanism. Many prokaryotic biominerals, in fact, do not follow such a model. Consistently, however, whether the paradigm applies or not, the organic macromolecules are formed first and they direct or induce the growth of specific minerals and their polymorphs. To this day, the organic macromolecular components have been identified in only a few biominerals. This paradigm, therefore, is to be interpreted as a conceptual mechanism, not as a detailed model of interaction between known molecules. The present chapter discusses the possibility of investigating the organic mineral interface, and the chemical bonds formed at that interface, in essence, zooming in on the interface as shown in Figure 3D.

In both biologically controlled and mediated biomineralization (Lowenstam 1981), the organic components are formed first, then these bind a few ions, which serve as nucleation sites for crystal growth (Lowenstam and Weiner 1989; Falini et al. 1996; Gotliv et al. 2005). Self-assembly and epitaxial crystal growth subsequently complete the composite structure discussed in Figure 3. We propose that the exploitation of such templation mechanisms can be
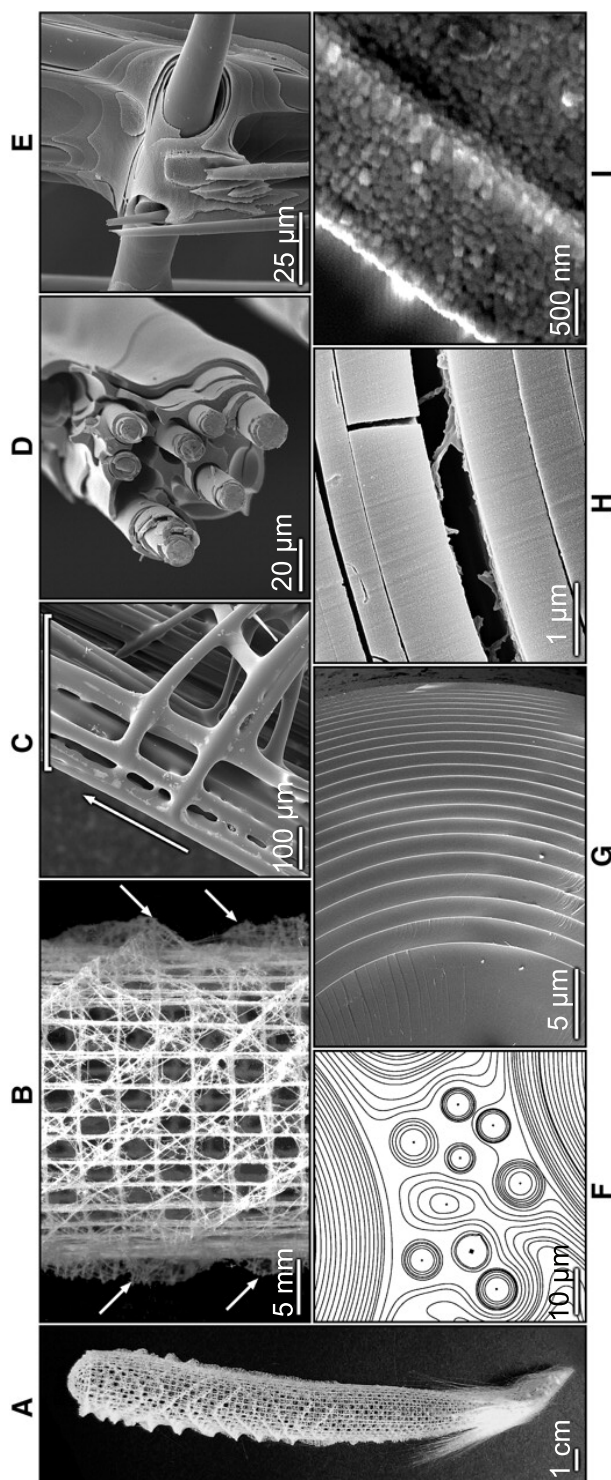
Figure 1. Structural analysis of the mineralized silica skeleton of *Euplectella* sp., a deep sea sponge from the Pacific Ocean. (A) Photograph of the entire skeleton, showing the cylindrical glass cage. (B) Fragment of the cage structure showing the square-grid lattice of vertical and horizontal struts with diagonal elements arranged in a chessboard manner. Orthogonal ridges on the cylinder surface are indicated by arrows. (C) Scanning electron micrograph (SEM) showing that each strut (enclosed by a bracket) is composed of bundled multiple spicules (the arrow indicates the long axis of the skeletal lattice). (D) SEM of a fractured and partially HF-etched single beam revealing its ceramic fiber-composite structure. (E) SEM of the HF-etched junction area showing that the lattice is cemented with laminated silica layers. (F) Contrast-enhanced SEM image of a cross section through one of the spicular struts, revealing that they are composed of a wide range of different-sized spicules surrounded by a laminated silica matrix. (G) SEM of a cross section through a typical spicule in a strut, showing its characteristic laminated architecture. (H) SEM of a fractured spicule, revealing an organic interlayer. (I) Bleaching of biosilica surface revealing its consolidated nanoparticulate nature. Reprinted with permission of AAAS, from Aizenberg et al. (2005), *Science,* Vol. 309, Fig. 1, p. 275-278.
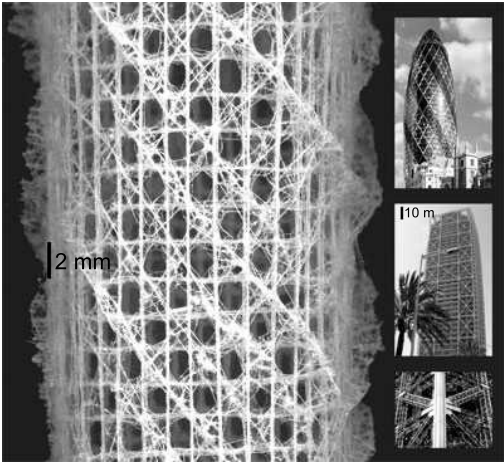
Figure 2. The *Euplectella* sp. Skeletal system structure (left) resembles that of the Swiss Re Tower in London (top right), the Hotel Arts in Barcelona (center right), and the Eiffel Tower in Paris (fragment shown bottom right). The characteristic structure with vertical and horizontal struts to form a checkerboard pattern, and diagonal struts at every other square is optimized for mechanical strength. Image courtesy of Joanna Aizenberg.
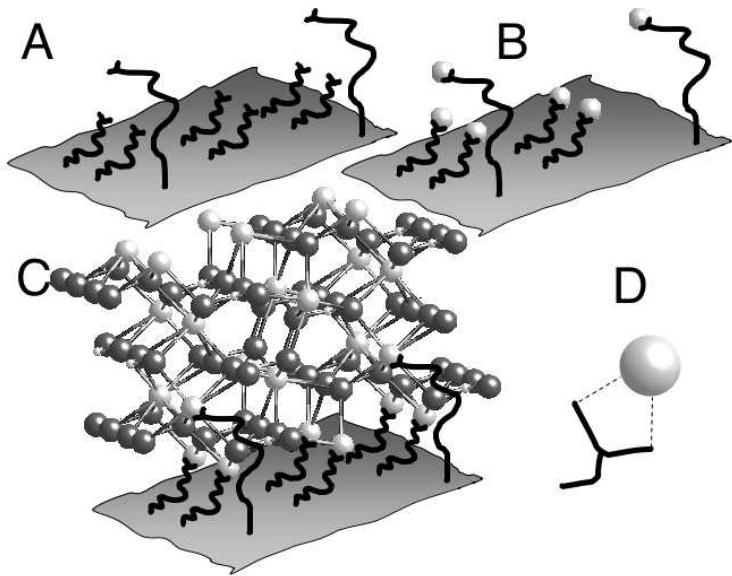

Figure 3. Paradigm for the epitaxial overgrowth, or templation, mechanism in biomineralization. The organic matrix (A) is composed of macromolecules, which depending on the particular biomineral may include a single organic molecule, e.g., a polysaccharide or a complex arrangement of proteins and glycoproteins. In all cases the organic components have charged functional groups that attract ions from solution (B). The steric arrangement of organic macromolecules, their sequence, and folding determines the precise position in three dimensions of the ions. Such positions are only compatible with a specific mineral, even more: they are only compatible with a well-determined polymorph of a specific mineral (C). The crystal structure shown (C) is aragonite, the large white ions in (B) are Ca^{2+}, while the small-white and large-dark atoms are C and O, respectively in (C). (D) Zooming in on the organic-mineral interface: the inter-atomic bonds are indicated by dashed lines. A similar mechanism of epitaxial overgrowth takes place in many matrix-mediated eukaryotic and some biologically induced prokaryotic biomineralization mechanisms.

considered a "genome shortcut", naturally selected for minimizing the amount of information the organism must transfer down the lineage, while maximizing the performance of the final composite material. Specifically, self-assembly and epitaxial crystal growth are harnessed by the organism, therefore the only information stored in the genome is that involving the synthesis of the organic macromolecules of Figure 3A.

Zooming in on the organic-mineral interface

Several authors suggested that the negatively charged amino acids, aspartate and glutamate, along their protein sequences attract positive ions from solution and initiate crystal nucleation and growth (Mann 2001; Weiner and Dove 2003; Gotliv et al 2005). Certainly the concentration of these amino acids in the known and sequenced organic matrix proteins is very high. They usually constitute between 30 and 40 mol% of the matrix protein, and in some cases even more. The recently discovered "Asprich" family of proteins from the bivalve mollusk *Atrina rigida* contain more than 50 mol% of aspartate and 10 mol% glutamate, hence their name (Gotliv et al. 2005). Therefore, the paradigm by which negatively charged amino acids collect ions from solution, provide the nucleation sites, and direct the epitaxial growth of biominerals deserves further investigation.

A novel set of tools is necessary to discover exactly which molecules interact at the organic-mineral interface, and at which specific molecular sites the first chemical bonds are formed, that is, how biogenic mineral formation begins. X-ray spectromicroscopy, used in combination with other microscopic and biological methods, is one such novel tool to explore the chemistry of templation mechanisms at this interface.

SPECTROMICROSCOPY OF BIOMINERALS

XANES spectroscopy of biominerals

Only recently has the study begun of templation mechanisms in biominerals using X-ray absorption near edge structure (XANES) spectroscopy. We believe that the understanding of organic-mineral templation can be significantly improved with XANES spectroscopy, because this powerful chemical analysis is sensitive to elemental composition, oxidation state, coordination number, and crystal or molecular structure and orientation of minerals and organic molecules (Stöhr 1992). XANES spectroscopy is a technique first introduced in the early 1980s—under X-ray illumination the sample emits electrons and photons, which constitute a spectrum as the X-ray energy varies. In this section a more detailed description will introduce the biomineralogist to this spectroscopy, to the microscopy version of it, and to the combination of spectroscopy and microscopy, termed spectromicroscopy.

The best tool for understanding the chemical and physical properties of any material is one that reports on the x,y,z coordinates of atoms in the material. This can be done with great accuracy (1 Å resolution) using X-ray diffraction on periodic structures, such as bulk mineral crystals or crystallized organic macromolecules, when these can be crystallized. For all other systems, which are not periodic—for example, organic macromolecules that cannot be crystallized—one is left with information that can be retrieved with spectroscopies. Various kinds of spectroscopies detect different characteristics of the specimen: the resonances of nuclei, the vibrational states, the electronic structure and many more. All these approaches are limited, compared to diffraction, but they are all that is available for the majority of organic molecules. XANES is one such spectroscopy, and a very powerful one compared to others, although not quite as informative as diffraction. Its main advantage is its wide range of applicability: it can in fact detect and report on the electronic structure of ordered and disordered materials, minerals surfaces, organic macromolecules, their molecular structure, composition, and the chemical bonds that these molecules form with minerals and nano-crystalline mineral precursors.

For a complete review of the XANES approach see Stöhr 1992. Briefly, XANES spectroscopy probes a specific element according to its absorption of X-ray photons, at energies that are characteristic of the element and the absorption edge. Absorption edges correspond to transitions between occupied atomic-like electronic shells (e.g., 1s, 2p, 3d, etc.) to unoccupied electronic states (molecular antibonding orbitals such as π*, σ*) that are strongly affected by both the absorbing atom itself and by its neighboring atoms. Transitions from the 1st(e.g., 1s), 2nd(e.g., 2s or 2p), 3rd, etc. atomic shells to molecular orbitals are called K- or L- or M-edges. These probe bonds of the absorbing atom to intra-molecular and, to a lesser degree, extra-molecular neighbors. For example the transition from 1s to π* of the C=O in the carboxyl group (COOH) has a distinct resonance (peak in the XANES spectrum) at 288.6 eV.

XANES spectroscopy can also detect the presence of specific bonds in molecules, and determine the orientation of molecules or functional groups on the surface of solids. Since the absorption edges of low-Z elements (up to atomic number Z = 30, including all non-gaseous elements from Li through Zn), which are the most relevant for biominerals, are in the 10-1000 eV range of binding energies, a source of photons with such energies must be used to observe such edges with XANES. The only tunable sources of 10–1000 eV photons, called the soft-X-ray range, are synchrotrons. Synchrotron radiation is also emitted by accelerated ions in the universe such as galaxies and nebulas, but those sources are too distant, their photon flux is therefore too low, screened by the atmosphere, and not easily tunable; therefore galaxies and nebulas are not useful as illuminating sources for XANES of materials on Earth. Thus, XANES spectra are acquired at synchrotron facilities while scanning the photon energy across the absorption edges of the relevant elements. When the photon energy reaches or exceeds the binding energy of electrons in a specific atomic shell, the sample photoemits, that is, it emits electrons by the photoelectric effect. The photoelectric effect was first observed by H. Hertz in 1887 (Hertz 1887); but only explained in 1905 by A. Einstein (Einstein 1905; the centennial celebration is undergoing this year). With his explanation Einstein introduced the concept of a photon, which is a quantum of electromagnetic energy. For this fundamental leap in the understanding of light and matter, and not for the more famous special and general relativity theories, Einstein earned the Nobel prize in 1921.

In an effort to avoid a quantum-mechanical presentation, we provide in Figures 4-6 an overview of all the information afforded by XANES, and provide via examples an introduction to this extremely powerful approach, tailored to entice the biomineralogist and the geomicrobiologist. Figure 4 illustrates the sensitivity of XANES spectromicroscopy to the elemental composition of samples, and the possibility of spatially mapping the elemental distributions. Figure 5 shows the sensitivity of XANES spectra to the oxidation states of two transition metals at the L-edges.

The dramatic differences introduced in the XANES spectral lineshape by changes in oxidation states make it possible to identify with this spectroscopy the chemical species present in the sample. By combining this information with the imaging capability demonstrated in Figure 4, the spatial distribution of elements and their oxidation states can be determined.

As mentioned above, XANES spectroscopy is also sensitive to the crystal structure. Figure 6 shows the difference in spectra acquired from $CaCO_3$ and ZnS mineral polymorphs, that is, minerals in which the chemical formula is identical but the crystal unit cell has a different arrangement. Slight differences in the local structural and electronic environment of elements in alternative crystal polymorphs can give clear fingerprints in XANES spectra.

XANES spectroscopy is also sensitive to coordination, that is, the number of atoms to which the element under analysis is bonded. Calcium in calcite is 6-coordinated, that is, each Ca atom is bonded to six oxygen atoms all at the same distance (2.35 Å). In aragonite Ca
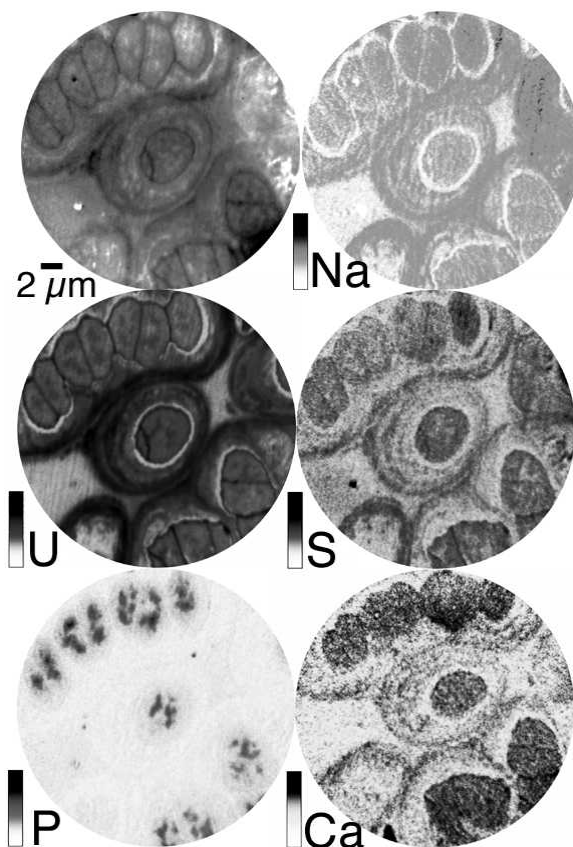
Figure 4. X-ray photoelectron emission spectromicroscopy (X-PEEM) image (top left) of *Calothrix* cyanobacteria embedded in epoxy and microtomed to a 60 nm thick section. In the top left portion of the field of view a *Calothrix* filament, containing seven bacteria, is visible, while at the center is the cross section of a single-cell, or possibly a filament extending along the direction perpendicular to the image. The distribution maps of sodium, uranium (from uranyl acetate stain), sulfur, phosphorus and calcium are also reported. The distribution maps were obtained by digital ratio of two images, on- and off-peak at the Na L-edge, U O-edge, S L-edge, P L-edge and Ca L-edge respectively, and represent the local concentration of the relevant element: darker gray levels indicate greater elemental density. Notice the high concentration of Na, S, U and Ca in the outer sheaths, and the high density of P corresponding to bacterial DNA. Sample courtesy of Susanne Douglas.

has 9-fold coordination, with five distinct bond lengths; these are: one oxygen at 2.32 Å, two oxygens at 2.43 Å, two oxygens at 2.51 Å, two oxygens at 2.57 Å and two oxygens at 2.66 Å. Consequently, the differences in the crystal field peaks (arrows in Fig. 6A) between aragonite and calcite may be due to both coordination and crystal structure. In both ZnS polymorphs, sphalerite and wurtzite, sulfur atoms are 4–coordinated (as are the Zn atoms), and the near-neighbor environments are almost identical. The crystal structures are different (cubic and hexagonal), therefore the distribution of atoms in the third and higher shell of atoms around the sulfur sites are distinct, and this is the origin of the spectral differences in Figure 6B.

XANES spectroscopy has been successfully used to reveal the presence and oxidation state of specific elements in geologic minerals (Sturchio et al. 1998), the structure of synthetic
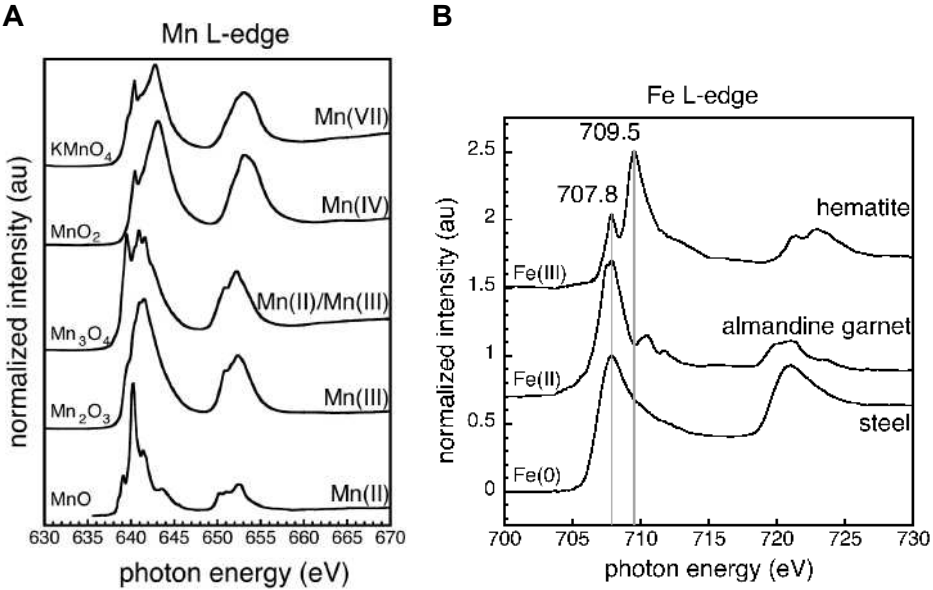
Figure 5. (A) Manganese L-edge X-ray absorption near edge structure (XANES) spectra of manganese oxides. The formal Mn oxidation states are given on the right. (Data from Gilbert et al. 2003a). (B) Iron L-edge XANES spectra from ferric (III), ferrous (II) and metallic iron (0), in the minerals and metal indicated. (Data from Frazer et al. 2005)
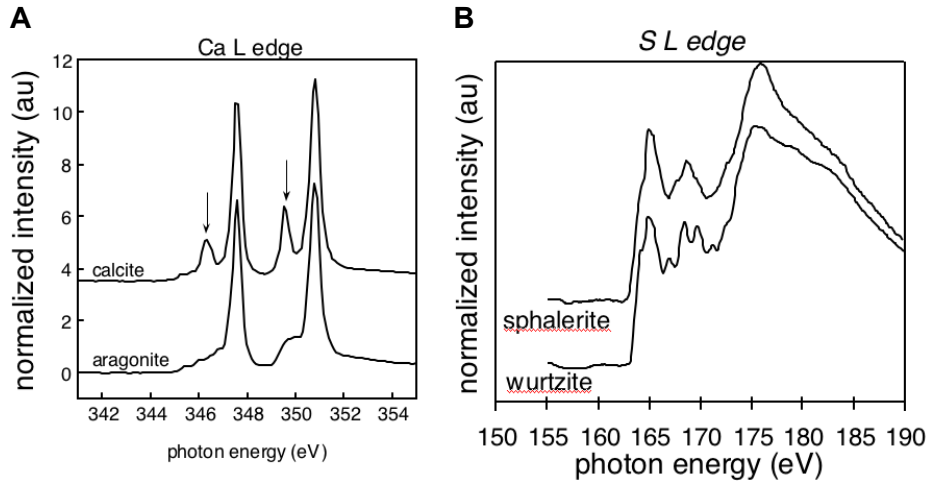

Figure 6. (A) Ca L-edge XANES spectra from calcite and aragonite, trigonal-rhombohedral and orthorhombic polymorphs of $CaCO_3$, respectively. The two main peaks, common to both spectra are the L_3 and L_2 edges, respectively. Two additional peaks at ~346 and ~350 eV (arrows), due to the crystal field, are prominent in calcite but have lower intensity and different line shape in aragonite. (B) XANES sulfur L-edge spectra from sphalerite and wurtzite, cubic and hexagonal polymorphs of ZnS, respectively. Notice the difference in line shape between 165 and 170 eV. Used with permission of the American Chemical Society, from Gilbert et al. (2003), *J. Phys. Chem. A*, Vol. 107, Fig. 1, p. 2839-2847.

materials (Bozek et al. 1990), elemental speciation in soils and sediments (Myneni et al. 1997; Beauchemin et al. 2003; Zawislanski et al. 2003) and other environmentally relevant samples (Myneni 2002a,b; Myneni et al. 1999).

Many other experiments on the microlocalization of trace elements in eukaryotic cells (De Stasio et al. 1993, 1996, 2001; Gilbert et al. 2000) and the identification of prokaryotic biomineral products (Labrenz et al. 2000; Lawrence et al. 2003; Lopez-Garcia 2003; Chan et al. 2004), also attest to the power and breadth of XANES spectroscopy and spectromicroscopy.

As mentioned, the lineshape of XANES spectra gives information on the molecular and/or crystal structures surrounding the element under analysis. The interpretation of spectral lineshape and peak assignment, however, can be complicated.

When the molecular or crystal structure is known, and relatively simple, *ab initio* calculations can be used to simulate the XANES spectrum. A comparison of experimental and calculated spectra enables peak assignment to specific molecular structures. Specific peaks can be considered "spectral signatures" of specific molecular features. XANES is extremely sensitive to carbon chemistry: examples of molecular features that generate well-established spectral signatures are C≡C, C=C, C–O, C=O, C–O, as well as C–C–C bond angles, conjugation of adjacent bonds, etc. A material that contains several of these molecular features exhibits a XANES spectrum resulting from the combination of their corresponding spectral signatures: the "building blocks" (Stöhr 1992).

For other edges, e.g., Si or S at the L-edge, simulations of XANES spectra are not currently adequate because the electronic structure is too complex to be calculated. In these cases, the spectral signatures do exist and are measurable, but they are not univocally assigned to specific bonds or molecular structures. Unknown minerals, however, such as sub-micron silicate inclusions, can still be identified by empirical comparison with spectra from known, macroscopic, reference silicate minerals (De Stasio et al. 2003; Gilbert et al. 2003b).

XANES microscopy of biominerals

XANES spectroscopy has been used to study the same kind of molecular interactions discussed hereafter, but without spatial resolution. Examples include organic-mineral interaction at the binding sites in metalloproteins (Benfatto et al. 2003) or between metal ion and humic macromolecules (Myneni et al. 1999; 2002a).

There are practical reasons that, until recently, completely precluded the spectromicroscopy of biomineralized structures, as described below first from a spectroscopy, then from a microscopy point of view.

XANES spectroscopy can be performed in two ways: by detecting either fluorescence photons or photoemission electrons (photoelectrons) from a solid sample surface. Fluorescence XANES signal is most intense for high Z elements (Z > 30). These elements have their core shell electrons at binding energies much greater than 1000 eV, therefore the corresponding absorption edges detectable by XANES spectroscopy can only be detected in the "hard-X-ray" regime. On the contrary, low Z elements, which include all the organic elements C, N and O, have their absorption edges below 1000 eV: the C K-edge is at 285 eV, the N K-edge at 400 eV, and the O K-edge at 531 eV. Since none of these edges is easily accessible to the hard-X-ray fluorescence range, the organic components of biominerals have never before been studied with fluorescence XANES.

Photoelectron XANES, also known as total electron yield or TEY-XANES, is much more intense than fluorescence below 1 keV, where the Si, P, S, and Ca L-edges, and the C, N and O K-edges are located. In this spectral region, a strongly space-averaged TEY spectroscopy

has always been possible on an insulating biomineral. This is, however, not particularly informative, given the highly organized microscopic structure of biominerals.

Spectromicroscopy with X-ray PhotoElectron Emission Spectromicroscope (X-PEEM) adds spatial resolution to the TEY-XANES experiment, down to the 10 nm level (Frazer et al. 2004). Until recently, however, X-PEEM could only image and analyze the chemistry of conductive sample surfaces. Insulating samples such as minerals and biominerals could not be analyzed without major charging problems.

Transmission X-ray microscopy experiments (e.g., scanning transmission X-ray microscopy, STXM (Kilcoyne 2003; Tyliszczak 2004), which do not suffer from charging, are limited to very thin solid samples (few atomic monolayers) or dilute liquid samples. Most biominerals, therefore, are excluded from this powerful analysis.

Overcoming charging effects

We recently optimized a differential-thickness coating method (De Stasio et al. 2003) that enabled us to extensively study mineral and biominerals surface with X-PEEM and do high-resolution imaging and XANES analysis on them (35 nm or better) (Gilbert et al. 2003-2). The coating approach is shown in Figure 7.

We have used this coating approach on a variety of insulators, including wood, quartz, zircons, glass slides, tribological polyphosphate and nano-diamond films, cells in culture, mollusk shells and bone. In all these cases the coating completely removed charging and enabled micro- and nano-XANES spectroscopy of insulators. Figure 8 shows a representative example of the results enabled by differential-thickness coating. As aforementioned, the combination of
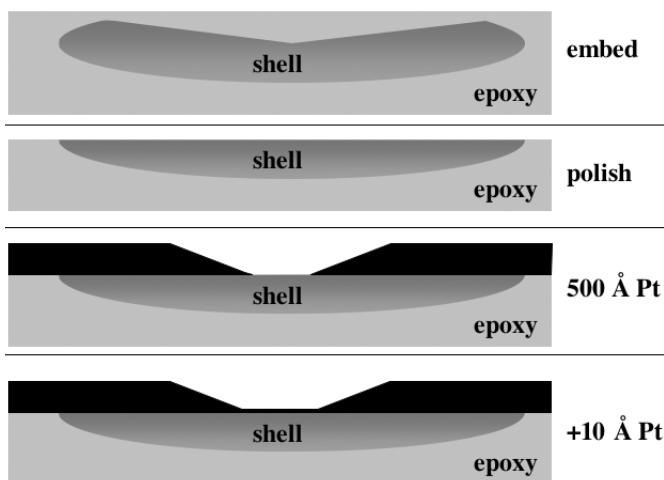

Figure 7. Schematic diagram showing the preparation steps (top to bottom) for the differential thickness coating. First the biomineral (e.g., a mollusk shell) is embedded in epoxy, then the surface is polished with grit, down to 50 nm if high-resolution imaging is desired, then a thick coating (500 Å) of platinum is deposited by magnetron sputtering on the sample, while masking and not coating the central area, typically 3 mm in diameter, which will then be analyzed by X-PEEM. Finally, a thin coating (10 Å) is deposited on the whole sample surface. The photoelectron escape depth is on the order of 30 Å at the C K-edge, therefore photoelectrons from the shell can be collected through the 10 Å coating at the center. The thicker coating layer around the central region ensures perfect conductivity and a good electrical contact with the sample holder, therefore the sample can be kept at a reliable and stable voltage, it does not charge when electrons are extracted by X-ray illumination, and XANES analysis can be performed (De Stasio et al. 2003).
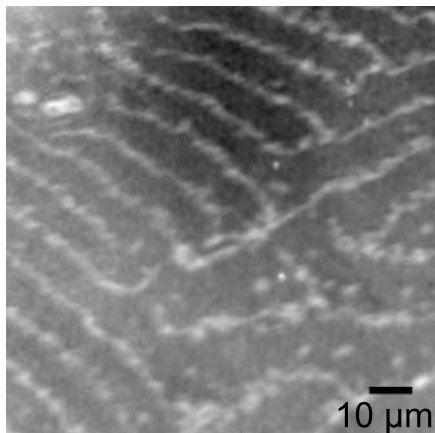
Figure 8. Distribution map of Ca in the nacreous layer of pinctada margaritifera, the Tahitian black pearl oyster. Dark indicates higher Ca concentration. The Ca-poor regions between nacre tablets are thicker organic matrix strata that could be due to seasonal changes, as suggested by other researchers of abalone nacre (Lin and Meyers 2005), although the thickness and spacing are different in pinctada. This map was acquired using the spectromicroscope for photoelectron imaging of nanostructures with X-ray s (SPHINX) instrument, which is an X-PEEM (Frazer et al. 2004), on a fragment of nacreous layer from pinctada embedded in epoxy and polished.

XANES spectroscopy and X-PEEM microscopy is called spectromicroscopy. From an image such as the one in Figure 8, specific regions of interest can be selected (with the computer mouse), and spectra (e.g., C K-edge XANES spectra) can be extracted, showing different spectroscopic signatures characteristic of the crystals and the organic matrix. This powerful technique can investigate both the organic and the inorganic components of biominerals.

Real-time, full-field imaging can be done with a maximum field of view of 180 µm in diameter. At this low magnification the area of interest in a biomineral can easily be identified, then zooming in to higher magnification down to a field of view of 1.7 µm allows high-resolution imaging and spectroscopic analysis of biomineral nanostructures. The usual mode of data acquisition consists of acquiring stacks of images while scanning the photon energy, therefore obtaining "movies" that can then be played independent of the synchrotron source. In these movies the third coordinate is energy rather than time, and each pixel (typically 512×512 pixels in each image) contains the full XANES spectrum. The number of spectra simultaneously acquired is therefore 2×10^5. The resulting complexity in data analysis and interpretation initiated a considerable effort in software design, which is in constant evolution.

From each one of these movies, all the elemental composition, oxidation state, coordination number, molecular or crystal structure information is available, and can be retrieved after data acquisition. Once carbon XANES spectra from the bound mineral-templating and unbound organic matrices of biominerals are obtained, the difference between those spectra reveals the organic-mineral interaction. Interpretation of the data is then done by comparison with the extensive literature on carbon XANES spectroscopy in individual amino acids and organic compounds (Stöhr 1992; Kaznacheyev et al. 2002; Carravetta et al. 1998; Myneni 2002b; Lawrence et al. 2003), or by comparison with reference molecules prepared and analyzed separately for a specific interaction.

Two main limitations remain for XANES spectromicroscopy with the X-PEEM approach: the samples must be compatible with ultra-high vacuum, and must be flat. The vacuum compatibility requirement arises from the necessity to collect photoelectrons, which would recombine with gas molecules if these were present in the experimental chamber. The flatness requirement arises from the necessity to keep the sample at high voltage (typically –20 keV) to accelerate electrons away from the sample surface and towards the electron optics column. If the samples have high surface corrugation, greater than ~1 µm, severe distortions of the electric field provoke imaging artifacts and distortions, and in extreme cases even arching and

sparking which preclude analysis. Surface corrugations lower than 0.5 μm in height, however, are very easy to obtain on solid samples such as minerals and biominerals by conventional surface polishing.

Another complication in the XANES X-PEEM approach is the difficulty in separating co-localized mixed phases. In the presence of multiple proteins in a biomineral (for example bone), carbon K-edge spectra may be too complicated to interpret. In that case it is necessary to acquire spectra from separate single-components and deconvolve individual contributions to XANES spectra of the mixture. Separation and/or purification of single components may not be possible. Furthermore, the components may not be spectroscopically distinguishable. If the individual organic components contributing to XANES spectra are known and spectroscopically distinct, singular value decomposition or cluster analysis methods can be used to deconvolve and quantify their contributions (Pickering et al. 2000; Lerotic et al. 2004).

THE ORGANIC-MINERAL INTERFACE IN MICROBIAL BIOMINERALS

Prokaryotic biominerals

Microbes or prokaryotic cells, which include Bacteria and Archea, are single-celled organisms. They are small, ranging in size from 200 nm to 7 μm, and lack the tissue differentiation and sophisticated external structures immediately apparent in single- and multi-celled eukaryotes. They also lack nuclei and membrane-bound internal organelles, with the notable exception of magnetosomes, surrounded by a phospholipid bilayer, in magnetotactic bacteria. Another exception are *Gemmatata obscuriglobus*, recently discovered bacteria with a double membrane surrounding their nucleoid, making them appear very similar to eukaryotes (Fuerst and Webb 1991; Lindsay et al. 2001). Prokaryotes, however, are among the most abundant organisms on Earth and can be found in virtually every known environment. In the driest location on Earth, the Atacama desert in Chile, 10^3 bacteria per gram of soil, can be found in the immediate underground (Maier et al. 2004). That number increases dramatically in more hospitable locations, up to 10^9 bacteria/g of soil in the rolling hills of Tuscany or the rain forests. Bacteria have also been found as deep under the Earth's crust as man has drilled: over 6000 m underground in a South African mine (Takai et al. 2001; Newman and Banfield 2002).

Prokaryotes not only inhabit all natural waters, soils and sediments, they are also capable of surviving in extremes of temperature, pH, or salinity. Additionally, unlike eukaryotes, which depend on glycolysis and require glucose as an energy source and oxygen as an oxidant, prokaryotes adapt to extract energy from diverse and often even multiple chemical reactions (Nealson and Stahl 1997). Sources of metabolic energy include redox reactions of minerals and ions in solution, as well as other inorganic molecules. One of the most eclectic of bacteria, *Shewanella putrefaciens*, can extract energy from reducing iron and manganese oxides, or sulfur, or fumarate or nitrate or many other compounds, in anaerobic conditions, depending on their availability. If oxygen is available instead, *Shewanella* becomes an aerobic organism using molecular oxygen to oxidize its energy source (organic carbon or hydrogen) (Myers and Nealson 1990).

Returning to the definitions of the different biomineralizations, microbes mostly perform biologically induced mineralization (Lowenstam 1981; Frankel and Bazylinski 2003). Magnetotactic bacteria are an exception, and are, together with coccoliths, the most studied microbes to exhibit biologically controlled mineralization (Bazylinski and Frankel 2003).

Biologically induced mineralization is especially significant for bacteria in anaerobic habitats, because in these conditions bacteria respire with sulfate and/or various metals as terminal electron acceptors in electron transport (Frankel and Bazylinski 2003).

Bacterial communities and biofilms thrive in environments rich in metal ions in solution and play an important role in mineral and/or rock dissolution, formation and deposition. From a materials science point of view, prokaryotes can be considered rock-catalysts: they enact or induce chemical transformations that lead to geochemical cycling and biomineral formation.

Minerals formed by biologically induced mineralization are generally nucleated and grown extracellularly as a result of metabolic activity of the organism and subsequent chemical reactions involving metabolic byproducts. Microbes secrete one or more organic macromolecules that react with ions or compounds in the environment, resulting in the subsequent deposition of mineral particles. This biomineralization may be unintended (Frankel and Bazylinski 2003) or advantageous for the organism (Chan et al. 2004). The minerals formed are often nanoparticles with considerable particle-size distributions (Frankel and Bazylinski 2003). A more thorough review of the general characteristics of prokaryotic nanoparticulate biominerals is given elsewhere in this volume (Gilbert and Banfield 2005).

As catalysts of biomineralization, however, prokaryotes are ideally configured. The larger the volume of an organism, the smaller the surface/volume ratio. Therefore the smallest organisms, microbes, are the most efficient in rapidly exchanging nutrients and waste byproducts with the surrounding environment. This metabolic advantage also implies that every bacterium can produce many times its body weight in biominerals. This efficiency has a price: bacteria, more likely than other larger organisms, are prone to become encrusted in their biomineral products. Furthermore, the microbial cell walls have a strong negative charge, with multiple sites available for metal binding. Metal ions in solution interact with the charged surface of the cell wall and initiate the formation of minerals. In other microbes, additional structures such as sheaths, capsules, S-layers and filaments provide binding and nucleation sites for mineralization. In addition, bacteria can induce mineralization by secreting *extracellular* polysaccharides and enzymes that, when released into the surrounding environment, transform minerals already present or induce the precipitation of new minerals and metastable mineral precursors. In the first case, the organic-mineral interface of Figure 3D is located on the surface of bacteria or on extruded but still connected structures, whereas in the second case the biomineralization occurs entirely extracellularly and away from the cell bodies. In both cases, the organic macromolecules induce nucleation and growth of the minerals, and are formed first. In prokaryotic biomineralization, however, a combination of the cell physiology and the chemistry of the surrounding environment determine the mineralization process and the final mineral product. No general statements, therefore, can confidently be made, and the paradigm of Figure 3A is certainly not widely applicable to prokaryotic biomineralization. The only general conclusion, perhaps, is that as a result of prokaryotic biomineralization the mineral changes redox state and the microbe gains energy, while in eukaryotic mineralization there is seldom a redox change, and the organism expends energy to form the biomineral.

The structure and dynamics of the microbe-mineral interface can be studied with atomic force microscopy (Lower et al 2001a). The interactions at that interface were also reviewed by Juniper and Tebo (1995). Several groups did spectroscopic analysis of the minerals formed by microbes. Among these, several studies used extended X-ray absorption fine structure (EXAFS) spectroscopy, which explores the structure of the 2-3 nearest neighboring shells of atoms in minerals of biogenic origin. These studies include Suzuki et al. (2002), Tebo et al. (2004), and Villalobos et al. (2005). Another article analyzed the changes in elemental concentrations between adhering and suspended bacteria using hard X-ray fluorescence spectromicroscopy (Kemner et al. 2004). Other studies used XANES or STXM-XANES spectromicroscopy, to analyze the oxidation states of biomineral products (Grush et al. 1996; Tonner et al. 1999; Toner et al. 2005). The latter studies, being all in the soft-X-ray region have the potential of analyzing both the mineral and the organic components of biominerals. This is, again, due to the location in energy of the absorption thresholds of organic elements, C, N, O, etc. However, to

the best of our knowledge all those studies have focused on the mineral components of bacterial biomineralization. We will later describe the first two cases in which the organic and mineral components, and the interface between them was analyzed using XANES spectromicroscopy (Chan et al 2004; Lawrence et al. 2003).

Biomineralization on various prokaryotic structures is reviewed hereafter, including cell walls, capsules, S-layers, sheaths, and filaments.

Bacterial cell walls

Bacterial cell walls can be classified into one of two groups based on their reaction to Gram's stain, a stain used for visible light microscopy. The cell walls of both Gram-positive and Gram-negative bacteria are negatively charged and may induce biomineral formation. However, Gram-negative cells have been shown to precipitate only a fraction of the quantity of minerals produced by Gram-positive cells (Beveridge and Fyfe 1985).

The cell wall for Gram-positive bacteria is made up of a layer of peptidoglycans and is separated from the interior of the cell by the plasma membrane. Peptidoglycans are composed of repeating dimers of N-acetylglucosamine and N-acetylmuramic acid. Each N-acetylmuramic acid molecule exhibits a side stem, which is a peptide with four or five amino acids. These stems covalently bond with other stems on neighboring peptidoglycan strands to form a strong and enduring 3-dimensional macromolecular structure that surrounds the bacterium. This cell wall is 15-25 nm thick (Fortin and Beveridge 2000). Both the glycan strands and peptide stems of peptidoglycans are rich in carboxyl groups and give the cell wall a net negative charge. Secondary polymers like teichoic or teichuronic acids, which contain negatively charged phosphoryl groups, are also bound in the peptidoglycan structure and increase the negativity of the cell surface. The large number of anionic reactive sites provided by the peptidoglycan layer is the main source of surface catalysis or mineralization in Gram-positive bacteria.

The cell walls of Gram-negative bacteria are more complex, both structurally and chemically. The peptidoglycan layer is much thinner than in Gram-positive cells (3 nm), contains no secondary polymers and is bound on both sides by membranes composed of lipid-protein bilayers. The outer membrane of Gram-negative bacteria is unique and asymmetric: the inner layer is composed of phospholipids but the outer layer contains an unusual lipopolysaccharide (LPS) layer, which is found uniquely in prokaryotes. LPS is a large complex molecule with three components: a lipid core, a core polysaccharide and a short polysaccharide chain that contains unique and species-specific sugar sidechains. The core polysaccharide is rich in anionic phosphate and carboxyl groups and gives the cell wall a net negative charge. The sugar sidechains can extend up to 40 nm from core polysaccharides and may also contain negatively charged carboxyl groups (Langley and Beveridge 1999). In contrast to Gram-positive bacteria, the peptidoglycan layer is not only considerably thinner, but also shielded by the outer membrane in Gram-negative bacteria. Metal ions in the environment, therefore, cannot reach the peptidoglycans, presumably by the same mechanism excluding the Gram stain, and the biomineralization site is constituted of the numerous phosphate and carboxyl groups in the LPS layer (Fig. 9).

Active cell metabolism can slow down biomineral formation on the cell wall. A clear example of this behavior is given by *Bacillus subtilis* cells. During metabolism, a membrane-induced proton motive force continuously pumps protons into the cell wall. Therefore metal ions must compete with protons for anionic cell wall sites, and the result is that these bacteria bind more minerals dead than alive (Urrutia et al. 1992).

Capsules

Both Gram-positive and Gram-negative cells can possess additional outer layers that also
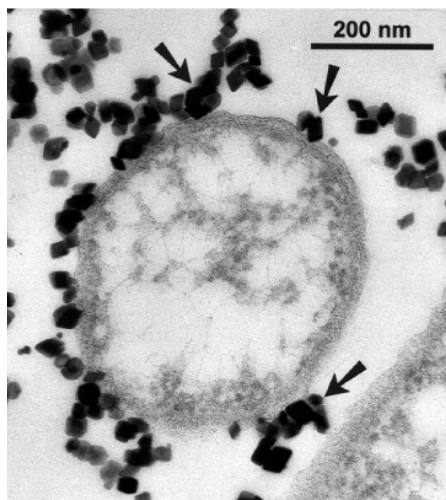
Figure 9. Transmission electron micrograph of *Shewanella putrefaciens*, a Gram-negative bacterium, exposed to nanocrystalline hematite. The crystals adhere to the cell wall due to its negative charge. This example illustrates that the bacterial cell wall not only binds ions from solution, but also already-formed mineral crystals. Reproduced with permission of the American Society of Microbiology, from Glasauer et al. (2001), *Applied and Environmental Microbiology*, Vol. 67, Fig. 5, p. 5544-5550.

induce biomineralization. Among these, capsules are highly hydrated amorphous matrices of exopolysaccharides or polypeptides, and strongly attached to the cell wall (see Fig. 10A). Capsules extend up to 1 µm away from the cell, and serve as protective shields for bacteria and, as cell walls, contain numerous carboxyl groups (see Fig. 10B). They contain 99 % water and allow for efficient transport of nutrients and waste products (Schultze-Lam et al. 1993).

The negatively charged polysaccharides filter and capture the positive cations from solution and induce precipitation away from the cell, thereby protecting the organism from becoming encrusted with minerals.
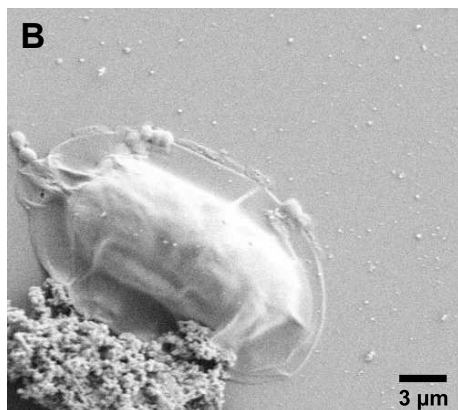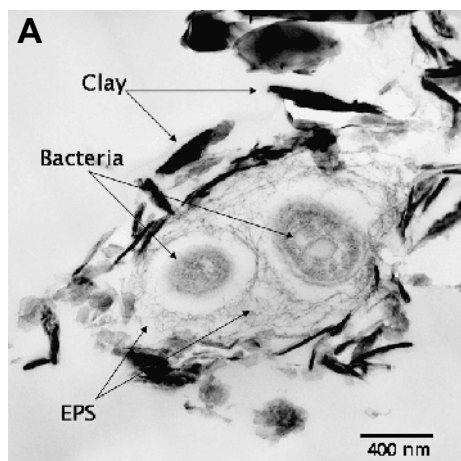

Figure 10. (A) TEM micrograph of bacteria, surrounded by exopolysaccharide (EPS) capsules, to which clay nanoparticles adhere. Reproduced with permission from *www.nwri.ca/envirozine/images/bacteria_e.gif.* (B) SEM image of another bacterium exhibiting the remains of a capsule. Bacteria in this ground water sample were not fixed, nor treated in any way, therefore the morphology of the 99% water-containing capsule is altered by dehydration. Sample courtesy of Clara S. Chan.

Capsules also stabilize the metal ion concentration around the cell wall. This is particularly advantageous when the metal ion concentration in the surrounding environment, which naturally fluctuates, reaches toxic levels. Experiments have shown that mutated forms of *Klebsiella aerogenes*, which do not produce capsules, were unable to survive in concentrations of metals in which the capsule-forming wild-type strains thrived (Bitton and Freihofer 1978).

S-layers

S-layers are paracrystalline surface layers 5 to 25 nm thick, containing many ordered repeats of a single protein or glycoprotein. Both Archea and Bacteria may form S-layers. These self-assemble into a well-ordered two-dimensional shell around the bacterium (Sleytr 1997). S-layer proteins or glycoproteins assemble into regular patterns in which the unit cell has 2-, 3- 4- or 6-fold rotational symmetry. The well ordered lattice contains pores that are identical in size and morphology. Since the S-layer becomes the outermost layer for the bacterium, it can serve several functions. In addition to determining the external morphology and shape of the cell, S-layers can be extremely resistant to external chemical challenges such as salts, detergents and even enzymes, and thus provide a protective armor for the cell (Schultze-Lam and Beveridge 1994). An S-layer with well-defined pore size is a barrier for compounds with a large molecular weight and therefore acts as a molecular sieve. S-layers may promote cell adhesion to crystalline surfaces and can also provide a method of surface recognition. Before S-layer formation, the proteins and glycoproteins forming this layer have negative charges, while after formation, as the proteins self-assemble into the ordered structure, the charged amino acids are embedded within the layer, and in most cases the final S-layer presents a net neutral charge at the cell surface. However, some S-layer proteins retain exposed anionic residues and are capable of inducing biomineralization (Schultze-Lam et al. 1993). The cyanobacteria *Synechococcus* spp, have a 6-fold symmetry S-layer as their outermost surface. This strain showed that strontium and calcium carbonates and other minerals can form on the S-layer (Fortin and Beveridge 2000).

Sheaths

Sheaths are well-defined biomineralized structures, such as hollow cylinders, that often surround chains of filamentous cells, and can be sites of biomineralization. Once biomineralized, the sheaths can remain long after the bacteria have died and decomposed. *Leptothrix* spp oxidizes ferrous iron in solution by secreting a complex matrix of heteropolysaccharides that catalyzes Fe oxidation and precipitation as iron oxyhydroxide (FeOOH) nanoparticles (Banfield et al. 2000). This bacterium thrives in high concentration of Fe and Mn, and leaves behind long sheaths as shown in Figure 11.

Filaments

Other bacteria induce the formation of biomineral filaments. The microbial mineral filaments of Figure 12 are formed by iron-oxidizing bacteria that have not yet been isolated nor phylogenetically identified. All these filaments show an unprecedented ~ 2 nm wide, up to 10 μm-long, curved pseudo-single crystals of akaganeite (β-FeOOH) in their cores (Chan et al. 2004), as presented in Figure 12B. The filaments are 20-200 nm wide, tangled, and composed of 2-line ferrihydrite (FeOOH·nH$_2$O), surrounding the akaganeite cores (Fig. 12B).

Formation of akaganeite in solution requires the presence of chloride, and is unexpected in fresh water. Chan et al. (2004) therefore suggested that akaganeite formation is catalyzed by organic polymers extruded by the bacteria. In this model, chemical bonds are formed between an organic molecule and ions in solution or amorphous nanoparticles, which are precursors of the crystal cores. As in other biominerals, the organic molecule acts as a template for a particular mineral polymorph, in this case, akaganeite. The paradigm of Figure 3A therefore
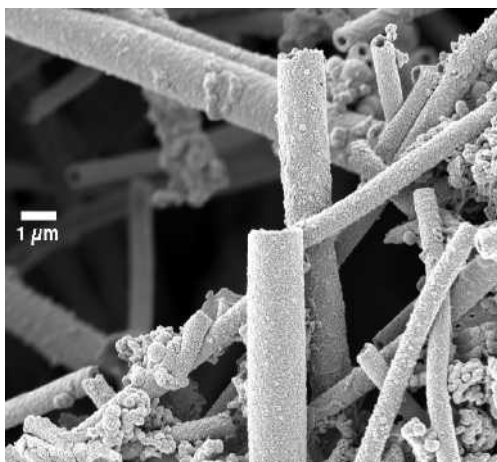
Figure 11. SEM micrograph of the FeOOH sheaths formed by *Leptothrix* spp in the Piquette mine, Tennyson, WI. Sample courtesy of Clara S. Chan.
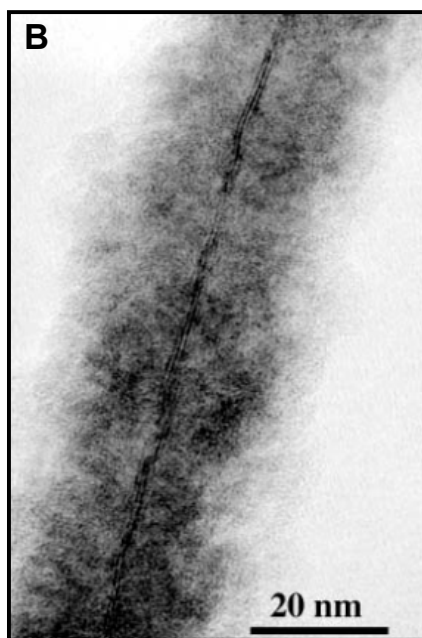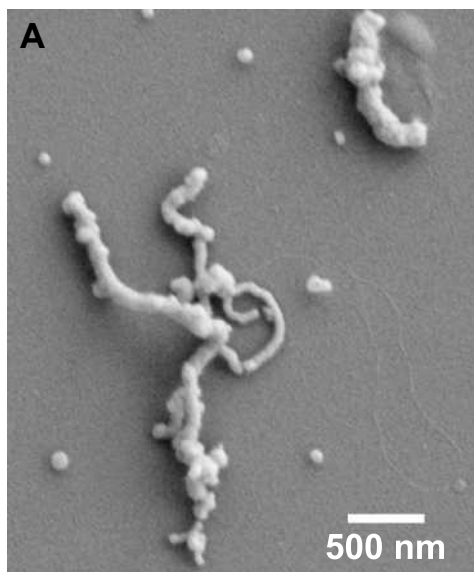

Figure 12. (A) SEM image of mineralized filaments produced by Fe-oxidizing bacteria in the Piquette abandoned and flooded mine in Tennyson WI. The filaments, approximately 100 nm in diameter are mineralized by FeOOH adhesion to the polysaccharide chains immediately after being extruded by the bacterium. On the right hand-side of the image a thinner, faint, strand is visible, possibly a non-mineralized polysaccharide fibril. Image used with permission of the American Journal of Science from De Stasio et al. (2005), *American Journal of Science,* Vol. 305, Fig. 4. Sample courtesy of Clara S. Chan. (B) TEM micrograph of a mineralized filament similar to the one in (A). The outer structure is formed by 1-2 nm wide 2-line ferrihydrite nanoparticles, while the central core of each filament exhibits a ~2 nm-wide crystalline core of akaganeite (β-FeOOH). This crystal core is only 2-3 unit cells wide, and can be identified as akaganeite by its distinctive crystal spacing (0.75 nm). Image courtesy of Jillian F. Banfield.

applies to this biomineral formation, although akaganeite crystal cores are formed upon aging of the mineral filaments, not as FeOOH nanoparticles are nucleated and grown.

Bacterially extruded polymer fibrils were analyzed using the SPHINX spectromicroscope, and identified as polysaccharides by comparison of their carbon K-edge XANES spectra with those from representative reference compounds (Fig. 13).

Mineralized filaments also revealed a polysaccharide spectrum at the carbon K-edge. FeOOH nanoparticles form a ~50 nm thick coating around the polysaccharide fibrils, hence the carbon signal is much lower, relative to the uncoated filaments.

Most interestingly, carbon spectroscopy from mineralized filaments revealed a new peak, which was absent from spectra of non-mineralized polysaccharide fibrils. This spectral signature was interpreted as a σ^* resonance of a C-O single bond involved in FeOOH binding. It is likely that the C-O groups that interact with FeOOH originate from the carboxyl groups $(O=C-O^-)$ of acidic polysaccharides (e.g., alginate). Acidic polysaccharides have an excess of COO^- groups that have high affinity for binding positive ions.

Chan et al. (2004) concluded that carboxyl groups in the unidentified biofilm polysaccharide chains must be the sites at which FeOOH amorphous nano-precipitates form chemical bonds, templating for the formation of akaganeite crystal cores upon aging (Fig. 13). This is a relatively simple biomineral, in which the biomineral composite has only three components: an unidentified COO^--rich polysaccharide, akaganeite crystal fibers and ferrihydrite nanoparticles. Because of its simplicity, its analysis (still incomplete) suggested a possible templation mechanism, which could be inferred at the molecular level (Chan et al. 2004).

Biomineralization of these bacterial filaments has common features with many other biominerals. As a careful reader may have already noticed in all the biominerals reviewed thus far, it is always negatively charged groups along the organic macromolecules that direct
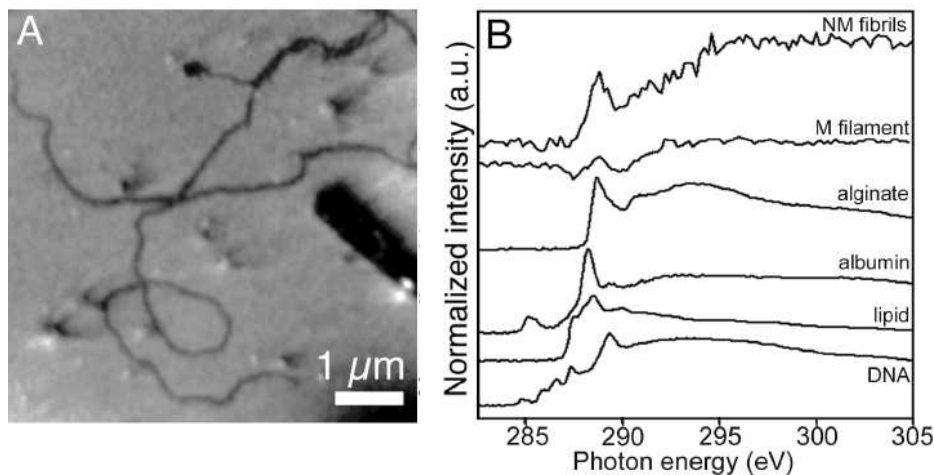

Figure 13. SPHINX image and spectra of the filaments produced by iron-oxidizing bacteria. (A) mineralized filaments from the biofilm-contain the akaganeite crystal core described in the text. (B) Carbon K-edge XANES spectra from non-mineralized (NM) fibrils and the mineralized (M) filament in (B), and reference organic molecules: alginate, albumin, lipid and DNA. Notice the similarity of the spectra from the NM fibrils and M filaments with the polysaccharide spectrum, and the additional structure in the one from the M filament: the peak at 292.4 eV was assigned to the C-O bond in carboxyl groups. Data from Chan et al. 2004.

the interaction with positively charged mineral ions, such as Fe^{3+} or Ca^{2+}. In the case of the microbial acidic polysaccharides, negatively charged COO^- groups are responsible. In cell walls, capsules, S-layers and sheaths, either acidic polysaccharides (rich in COO^- groups) or peptide sequences rich in negatively charged amino acids (also exhibiting carboxyl groups) enact the nucleation and biomineral growth. The paradigm of Figure 3, therefore, has one more identified component: at the interface of the inorganic and mineral components is most frequently, perhaps always, a carboxyl group.

We will now discuss the biomineralization paradigm in eukaryotes, and highlight the similarities of the core mechanisms.

THE ORGANIC-MINERAL INTERFACE IN EUKARYOTIC BIOMINERALS

Eukaryotic biominerals

The majority of animals mineralize at least part of their bodies, usually as internal skeletons or external armors, using a variety of proteins and minerals with calcium carbonates, calcium phosphates, and silica being the most common (Currey 2005). Other eukaryotic biominerals contain a variety of elements, including barium, strontium, iron, manganese, magnesium, copper, zinc, and sulphur. These complex composites, often hierarchically organized, include bone, teeth, eggshell, mollusk shells, crustacean shells, corals, sponge skeletons, the statoliths through which trees sense gravity and grow vertically even on the steepest mountain slopes, the otoliths in the inner ear of most animals, from humans to zebra fish (Söllner et al. 2003), warm jaws (Lichtenegger et al. 2002), and many more composites, in excess of 70 biominerals known nowadays. See Weiner and Dove (2003) and Mann (2001) for the most recent complete lists of biominerals.

Eukaryotic biominerals can be distinguished from their abiotic counterparts because of their uniform crystal size and habit and the regular nanostructures that result from biologically controlled mineralization (Weiner and Dove 2003). The control, again, is enacted by the organic matrix and its macromolecules: proteins, glycoproteins, and carbohydrates.

Mollusk shells, and in particular that of red abalone (*Haliotis rufescens*), have been widely studied for their very regular repeating crystalline domains and astounding properties. The nacre layer, or mother of pearl, at the inner surface of the abalone shell has a fracture resistance 3000 times greater than that of aragonite, the pure mineral of which it is composed. The toughening effect is due to well-defined nanolayers of organics at the interfaces between micro-tiles of aragonite (Kamat et al. 2000; Currey 2005). In nacre and many other eukaryotic biomineral structures, the stiff mineral tiles absorb the bulk of the externally applied loads. The alternating organic layers, in turn, provide toughness, prevent the spread of the cracks into the interior of the structure, and even confer a remarkable capacity for recovery after deformation (Smith et al. 1999). Two other structural characteristics of eukaryotic biominerals contribute to the superior mechanical properties of skeletons made from them. First, at the lowest level, they are often made of tiny crystals that are smaller than the "Griffith length" necessary for cracks to spread (Gao et al. 2003). Second, the precision with which they can be laid down (changing their main orientation over a few micrometers, for instance) allows exquisite adaptations to the loads to which the skeletons are subjected (Currey 2005).

Nacre is composed of approximately 95 mass percent aragonite and 5 mass percent organic macromolecules. We note that various groups have studied other systems of marine biominerals. For instance, in studies on marine sponges such as Tethya aurantia that form silica needles, research has focused on the role of the proteins and their possible use in organosilicon chemistry. The ultimate goal there is to manufacture silicon based polymeric materials in milder

conditions than those used in today's industry. The proteins responsible for biological silica synthesis have received a lot of attention recently, including their very own name, "silicateins" (Shimizu et al. 1998; Shimizu and Morse 2000; Weaver and Morse 2003; Pozzolini et al. 2004). In this section, we will focus on nacre and promote our opinion that the key to nacre formation lies at the organic-mineral interface. Understanding the role of that interface is thus pivotal to the development of biomimetics, that is, the field that imports biologically inspired concepts and mechanisms into the design and fabrication of new materials.

The nano-structure of nacre

Mollusk shell and pearl nacre presents a highly regular brick and mortar arrangement in which aragonite tiles, 500 nm thick along the *c*-axis, 10-20 μm wide along the a and b axes (Mann 2001), and polygonal in shape, form extremely flat layers (Fig. 14). Subsequent layers of aragonite tiles and organic matrix, composed of silk-like proteins and glycoproteins, keep alternating across the entire thickness of the nacreous layer (Currey 1977; Jackson et al. 1988; Schäffer et al. 1997).

The regularly repeating layering of nacre, the semi-transparency of aragonite and the pitch of this periodic structure (500 nm), which falls in the middle of the visible light wavelength range (400-700 nm), all combine to generate the iridescence typical of mother of pearl. As the observation angle varies, the color perceived changes due to the variation in apparent spacing between the semi-transparent layers of crystals. Furthermore, there is considerable crystallographic alignment, with the *c*-axes of most tiles lying in the direction perpendicular to the tiled planes. Aragonite is an orthorhombic polymorph of $CaCO_3$, whereas the outer prismatic layer of all mollusk shells is formed by columns of the trigonal-rhombohedral calcite polymorph. In the prismatic layer the *c*-axes are along the long axis of each prismatic column, perpendicular to the shell surface and parallel to the nacreous layer *c*-axes. Epithelial cells form a layer along the inner surface of the shell, called mantle, and secrete all the macromolecules of the organic matrix (see Figs. 15 and 16).

Mechanically nacre is stiff and resistant to fracture; it therefore combines the behavior of flexible materials that can absorb energy by rearranging their molecular conformation (distortion and deformation), and that of hard and stiff materials. On the other hand, it does not suffer from the limitations of its components, as it is neither compliant (as most soft materials)
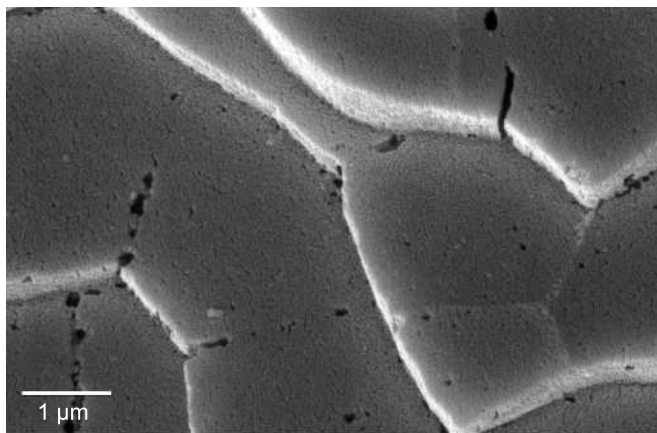

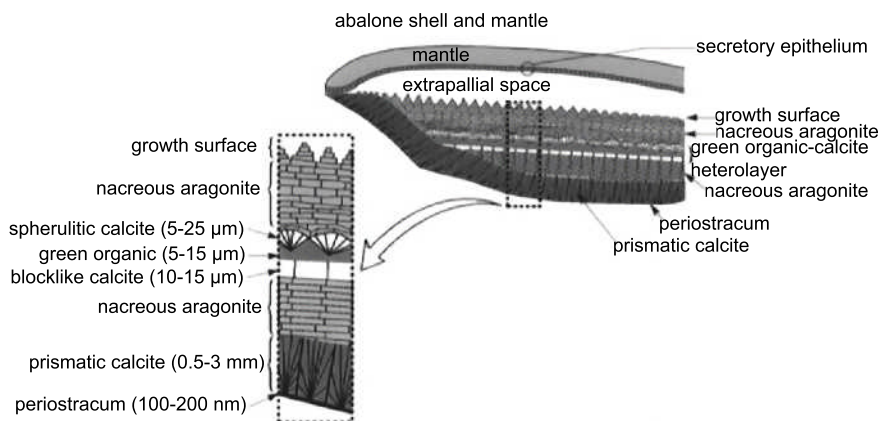**Figure 14.** SEM micrograph of red abalone nacre tiles seen at a fractured edge.

Figure 15. Schematic, not to scale, of a vertical cross-section of the outer edge of the shell and mantle of red abalone (Haliotis rufescens) with an enlargement indicating the thickness of each shell structure. The size of the extrapallial space is exaggerated for clarity. Used by permission of the American Chemical Society, from Zaremba et al. (1996) *Chemistry of Materials*, Vol. 8, Fig. 1a, p. 680.
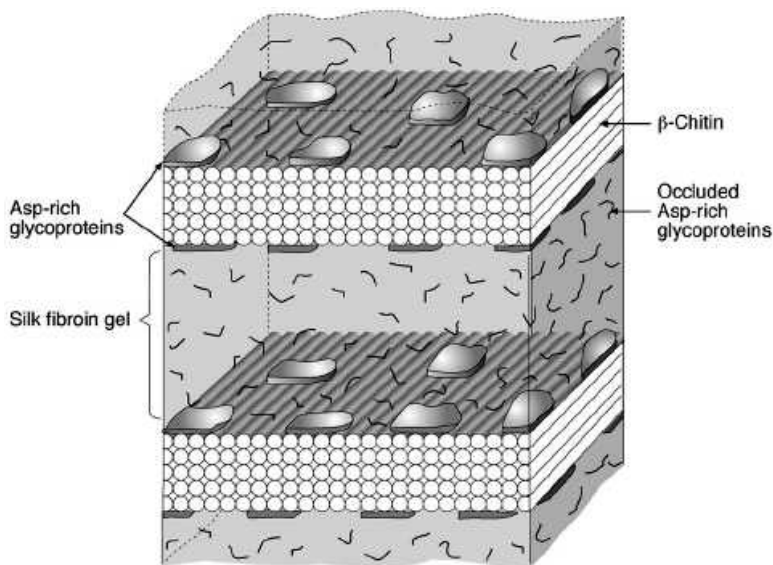

Figure 16. A proposed model for the organic matrix structure in nacre of the bivalve shell Atrina serrata, observed in the hydrated state by cryo-TEM. Note that silk was found to be present in both phases, the water-soluble and water-insoluble matrices. Reproduced with permission of Elsevier, from Levi-Kalisman et al. (2001), *J. Structural Biology*, Vol. 135, Fig. 1, p. 8-17.

nor brittle (as most hard materials). Jackson et al. (1988) reported the Young's modulus of nacre in the bivalve *Pinctada umbricata* to be approximately 70 GPa and 60 GPa for dry and wet samples, respectively, whereas the tensile strength is a corresponding 170 MPa and 140 MPa. The work of fracture varies between 350 and 1240 J/m^2 (up to 3000× higher than that of $CaCO_3$) (Jackson et al. 1988).

Interestingly, the organic layers are thick along the *c*-axis, very thin and hard to detect, or non-existent on the lateral surfaces of tiles (see Fig. 16). The thick organic layers between tile layers are consistent with the model in which sliding of the tiles give nacre its resistance to fracture (Lin and Meyers 2005). It is conceivable that upon sliding, the chains of looped organic macromolecules stretch and break loops without breaking the main molecular chain, thus conferring nacre with its elastic behavior (Smith et al. 1999).

Start and stop signals in nacre growth

Several groups studied the growth of abalone nacre and other mollusks (Addadi and Weiner 1985; Lowenstam and Weiner 1989; Belcher et al. 1996; Zaremba et al. 1996; Lin and Meyers 2005). In nacre the organic matrix is a true matrix: its continuous sheets are formed first (Fig. 3A) and they provide the many nucleation sites, which initiate crystal growth to fill the voids in the three-dimensional organic matrix. This the "start" signal. The position and nature of the nucleation points determines the crystal species and polymorph (Falini et al. 1996), while the structure of the voids in the matrix, presumably, determines crystal habit and size. Laterally, along the *a* and *b* axes, crystal growth is stopped by crystal-crystal contacts. At the surface of nacre, which is the growth front, tiles are piled up as stacks of coins, or cones, or Christmas trees, as many authors have called them (see Fig. 15). Lateral growth along the *a* and *b* (in plane) directions occurs in these cones until adjoining terraces come in contact. This is one of the "stop" signals, and explains the polygonal appearance of nacre tiles. Vertically, however, the reproducibly perfect thickness of 500 nm must be controlled by another extremely accurate "stop" signal, transduced by the preformed matrix macromolecules. Such signals, and the matrix molecules involved in the growth cessation, are still unknown (Lowenstam and Weiner 1989).

Since the aragonite tiles have a relatively small thickness in the *c* direction (the pure mineral aragonite crystals are much more elongated along that direction, and are much longer than 500 nm), there must be a signal stopping this growth. This signal may be linked to *stereochemical* adsorption of proteins in the growth of calcite crystals demonstrated by Addadi and Weiner (1985) and Addadi et al. (1987). It can be speculated that the host animal produces the proteins that stop growth in a periodic manner (Lin and Meyers 2005).

Another relevant observation is that the size of the aragonite tiles does not depend on the size of the animal.

The growth of nacre in space and time has been analyzed *in vivo* and *in vitro* using the *flat pearl* system (Fritz et al. 1994). They found that nacre growth begins with the secretion of proteins that mediate the precipitation of calcite. Other proteins then induce a phase transition from calcite to aragonite (Zaremba 1996; Belcher and Gooch 2000; Lin and Meyers 2005).

Some of the matrix macromolecules involved in nacre formation have been identified. Among the known molecules are the insoluble β-chitin central sheet in each organic matrix layer (Addadi and Weiner 1985), insoluble silk fibroin protein layers above and below this sheet, and unidentified soluble acidic macromolecules. Even without identification, however, these macromolecules can be extracted from nacre, exposed to non-shell β-chitin and silk fibroin in a saturated solution of $CaCO_3$ and induce nucleation and growth of aragonite, *not calcite* (Falini 1996). Aragonite formation is induced by the macromolecules even when seeding calcite crystals! (Thompson et al. 2000). This is particularly clear proof of the role of these unknown acidic macromolecules in polymorph selection, since aragonite is much less stable than calcite. The Thompson et al. (2000) experiment proves that nucleation and polymorph selection are independent in nacre formation. The recent discovery and sequence of Asprich proteins contributes to the clarification of the nature of these acidic macromolecules (Gotliv et al. 2005). Again, as already noted in microbial biominerals, it is the negatively

charged amino acids aspartate and glutamate in acidic glycoproteins in mollusk shell that are believed to initiate biomineral formation (Mann 1988, 2001; Mann et al. 2000; Weiss et al. 2000; Weiner and Dove 2003; Gotliv et al. 2005).

Stereochemical recognition determines the specific interactions between aspartic acid-rich proteins and certain faces of various calcium dicarboxylate crystals, which are used as model systems. The specific faces have carboxylate groups oriented perpendicular to the face and can therefore optimally complete the coordination polyhedron around the protein bound calcium ions (Addadi and Weiner 1985). A more recent study, which explored the subtle links between atomic scale dynamics and macroscopic crystal faces, clarifies further this issue and reconciles the *stereochemical recognition* model with the simple mechanistic model of crystal growth by step propagation across crystallographic faces, the *terrace-ledge-kink* model (De Yoreo and Dove 2004). A possible *stereochemical recognition* model for abalone nacre is reported in Figure 17.

Synergy of mechanisms for nacre growth

Several mechanisms likely conjoin in the formation of nacre. These are:

- Heteroepitaxial nucleation: in this case nucleation and growth of each aragonite tile are detrmined by the organic matrix sheet beneath it (Schäffer et al. 1997).
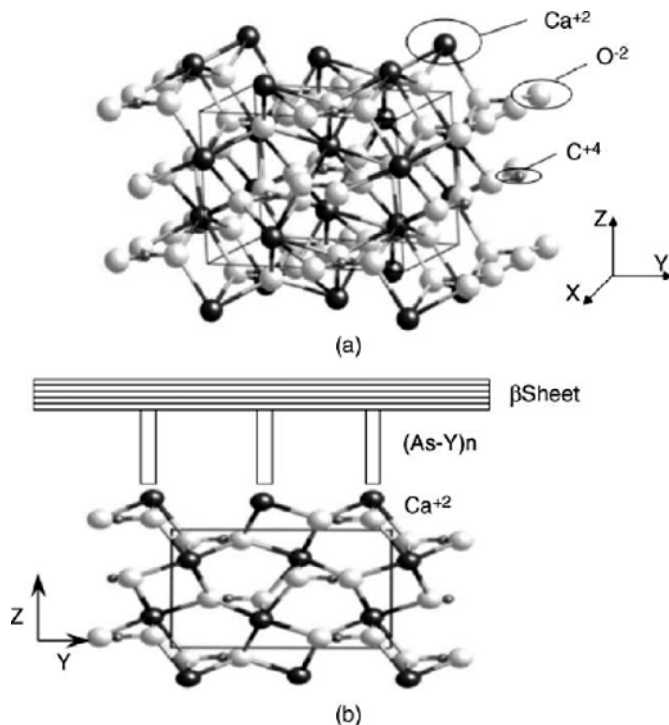

Figure 17. Unit cell of aragonite: (a) perspective view (b) normal view showing schematic position of (Asp-Y)$_n$ and β-pleated organic matrix sheet. Notice protruding Ca ions on (001) face: black atoms are Ca, small black are C and gray are oxygen. This model is in perfect agreement with the paradigm of Figure 3. Reproduced with permission of Elsevier, from Lin and Meyers (2005), *Materials Science & Engineering*, Vol. 390, Fig. 5, p. 27-41.

- Epitaxial crystal growth of the ith crystal layer, connected to the $(i − 1)^{th}$ crystal layer by mineral bridges. In this case the crystal would be uninterrupted across different tiles (Schäffer et al. 1997).

- After nucleation on the organic matrix sheet, the growth of aragonite may be mediated or catalyzed by proteins *in solution* (Falini et al. 1996).

All of these mechanisms, and possibly others not yet discovered, are likely to control in synergy the growth and architecture of nacre..

BIOMINERAL GLUE: THE CARBOXYL GROUP.

We have already highlighted the similarity of all organic-mineral interface in prokaryotic biominerals. In the few biominerals thus far analyzed at the molecular level, including prokaryotic and eukaryotic, it is often negatively charged carboxyl groups (COO^-) that attract positive ions from solution, and these nucleate for biomineral crystal growth. The carboxyl groups are located either along polysaccharide chains or in acidic amino acids, along the sequences of protein and glycoprotein rich in aspartate or glutamate (Mann 1988, 2001; Mann et al. 2000; Weiss et al. 2000; Weiner and Dove 2003; Gotliv et al. 2005). The very reason the latter are commonly called aspartate and glutamate, and not aspartic and glutamic acid, highlights the fact that they are nearly always deprotonated, and therefore their carboxyl group terminations are negatively charged at physiological pH (the typical pK for both is 4.4; Stryer 1995).

Carboxyl-group-rich proteins and/or polysaccharides are the most common and most effective cation-binding macromolecules that any organism can assemble to bind mineral precursors and either control or induce biomineralization. We hypothesize that this is why this molecular functional group was selected in many biominerals as the organic-mineral interface of Figure 3D. In this hypothesis, the carboxyl group is a molecular "glue" of choice for biominerals.

Interestingly, even when this hypothesis is not confirmed in specific biominerals, by analyzing with XANES an intact and pristine biomineral from both the mineral and the macromolecule perspective, it is always possible to identify spectral signatures, even if the bond sites and functional groups involved are not those expected.

CONCLUSION

Frequently in biology a gene or a protein is identified but its function is unknown for decades. Even now, in the most intensely studied genomes, 25% or more of the genes are yet to be associated with a function. In biomineralization it is quite the contrary: most often the function, namely, the formation of a specific biomineral structure is identified, but the molecule or molecules responsible for it are unknown. We know, however, that composite biominerals form as a result of complex chemical interactions between organic and inorganic matrices, and that the former acts as a template for the latter, according to a paradigm presented in Figure 3. Few approaches enable the simultaneous analysis of both the organic and mineral components in biominerals and their interface. XANES spectromicroscopy studies of that interface might reveal some of the molecular details of templation mechanisms (e.g., Figs. 13 and 17).

We note that at this interface, in diverse eukaryotic and prokaryotic biomineralization, there is frequently a carboxyl group. Acidic amino acids or polysaccharides with excess carboxyl groups are the most common and most effective cation-binding chemical species that any organism can assemble to bind mineral precursors and initiate templation. In this sense COO^- is a biomineral preferred "glue".

Ultimately, once the molecular-scale chemistry of the interface is elucidated in more biominerals, it may be possible to harness it and synthesize novel biomimetic composite materials that self-assemble and, as natural biominerals, outperform the sum of their components.

Two conceivable avenues towards bio-inspired synthetic materials are: (i) templation by structured organic surfaces, such as self-assembled monolayers or Langmuir-Blodgett films and functionalized polymers; and (ii) precipitation from solution with growth modifiers, such as ions, proteins, and synthetic polymers (Han and Aizenberg 2003).

The first biomineral-inspired man-made material synthetically reproduced the nacre assembly with alternating organic and inorganic matrices, using synthetic organic molecules and clay crystals. Remarkably, the tensile strength of the prepared multilayers was similar to that of nacre, and the Young's modulus approached that of lamellar bone (Tang et al. 2004). We envision a future with many more of these synthetic materials, assembling and structuring themselves at different scales as biominerals have done for well over 500 million years. Impact resistant cars, trains and spacecrafts, in which cracks do not propagate might one day have an attractive mother of pearl luster.

In the meantime, the best we can do is to analyze and understand at the molecular level the formation mechanisms of biominerals. The paradigm introduced here includes some prokaryotic and many eukaryotic biomineralization mechanisms. In prokaryotic biominerals, however, the organic components are fewer and simpler to analyze, while the mineral diversity is enormous. This is a distinct advantage offered by prokaryotes for understanding biomineral formation. Following that paradigm as an incomplete but useful starting point, and analyzing as many prokaryotic biominerals as possible, we anticipate that the mechanisms of biomineral formation will be further elucidated. The general rules, the exceptions and the anomalies that are characteristic of the living world will eventually be clear for the biomineral world.

ACKNOWLEDGMENTS

REFERENCES

Addadi L, Moradian J, Shay E, Maroudas NG, Weiner S (1987) A chemical model for the cooperation of sulfates and carboxylates in calcite crystal nucleation: relevance to biomineralization. Proc Natl Acad Sci USA 84:2732-2736

Addadi L, Weiner S (1985) Interactions between acidic proteins and crystals: stereochemical requirements in biomineralization. Proc Natl Acad Sci USA 82(12):4110-4114

Addadi L, Weiner S (1997) Biomineralization: a pavement of pearl. Nature 389:912-915

Aizenberg J, Weaver JC, Thanawala MS, Sundar VC, Morse DE, Fratzl P (2005) Skeleton of *Euplectella* sp.: structural hierarchy from the nanoscale to the macroscale. Science 309:275-278

Banfield JF, Nealson KH (eds) (1997) Geomicrobiology: Interactions Between Microbes and Minerals. Reviews in Mineralogy, Volume 35. Mineralogical Society of America, Washington D.C.

Banfield JF, Welch SA, Zhang H, Thomsen-Ebert T, Penn RL (2000) Aggregation-based crystal growth and microstructure development in natural iron oxyhydroxide biomineralization products. Science 289:751-754

Bazylinski DA, Frankel RB (2003) Biologically controlled biomineralization in prokaryotes. Rev Mineral Geochem 54:217-247

Beauchemin S, Hesterberg D, Chou J, Beauchemin M, Simard RR, Sayers DE (2003) Speciation of phosphorus in phosphorus-enriched agricultural soils using X-ray absorption near-edge structure spectroscopy and chemical fractionation. J Environ Qual 32(5):1809-1819

Belcher AM, Gooch EE (2000) Protein components and inorganic structure in shell nacre. *In*: Biomineralization. Baeuerlein E (ed) Wiley-VCH, Weinheim, Germany, p 221–249

Belcher AM, Wu XH, Christensen RJ, Hansma PK, Stucky GD, Morse DE (1996) Control of crystal phase switching and orientation by soluble mollusk-shell proteins. Nature 381:56-58

Benfatto M, Della Longa S, Natoli CR (2003) The MXAN procedure: a new method for analysing the XANES spectra of metalloproteins to obtain structural quantitative information. J Synchro Radiat 10:51-57

Beveridge TJ, Fyfe WS (1985) Metal fixation by bacterial cell walls. Can J Earth Sci 22:1893-1898

Bitton G, Freihofer V (1978) Influence of extracellular polysaccharide on the toxicity of copper and cadmium toward *Klebsiella aerogenes*. Microb Ecol 4:119-125

Bozek JD, Bancroft GM, Cutler JN, Tan KH (1990) Vibrationally resolved core-level photoelectron spectroscopy: Si 2p levels of SiH_4 and SiF_4 molecules. Phys Rev Lett 65(22):2757-2760

Carravetta V, Plashkevych O, Ågren H (1998) A theoretical study of the near-edge X-ray absorption spectra of some larger amino acids. J Chem Phys 109:1456-1464

Chan CS, De Stasio G, Welch SA, Girasole M, Frazer BH, Nesterova MV, Fakra S, Banfield JF (2004) Microbial polysaccharides template assembly of nanocrystal fibers. Science 303:1656-1658

Currey JD (1977) Mechanical properties of mother of pearl in tension. Proc R Soc Lond B 196:443-463

Currey JD (2005) Hierarchies in biomineral structures. Science 309:253-254

De Stasio G, Casalbore P, Pallini R, Gilbert B, Sanita F, Ciotti MT, Rosi G, Festinesi A, Larocca LM, Rinelli A, Perret D, Mogk DW, Perfetti P, Mehta MP, Mercanti D (2001) Gadolinium in human glioblastoma cells for gadolinium neutron capture therapy. Cancer Res 61:4272-4277

De Stasio G, Dunham D, Tonner BP, Mercanti D, Ciotti MT, Coluzza C, Perfetti P, Margaritondo G (1993) Aluminum in rat cerebellar neural cultures. Neuroreport 4:1175-1178

De Stasio G, Frazer BH, Gilbert B, Richter KL, Valley JW (2003) Compensation of charging in X-PEEM: a successful test on mineral inclusions in 4.4 Ga old zircon. Ultramicroscopy 98:57-62

De Stasio G, Mercanti D, Ciotti MT, Droubay TC, Perfetti P, Margaritondo G, Tonner BP (1996) Synchrotron spectromicroscopy of cobalt accumulation in granule cells, glial cells and GABAergic neurons. J Physics D29:259-262

De Stasio G, Schmitt MA, Gellman SH (2005) Spectromicroscopy at the organic-inorganic interface in biominerals. Am J Sci 305:

De Yoreo JJ, Dove PM (2004) Shaping crystals with biomolecules. Science 306:1301-1302

De Yoreo JJ, Vekilov PG (2003) Principles of crystal nucleation and growth. Rev Mineral Geochem 54:57-93

Einstein A (1905) Über einen die Erzeugung und Verwandlung des Lichtes betreffenden heuristischen Gesichtpunkt (On a Heuristic point of view about the creation and conversion of light). Annalen der Physik 17:132-148

Falini G, Albeck S, Weiner S, Addadi L (1996) Control of aragonite or calcite polymorphism by mollusk shell macromolecules. Science 271:67-69

Fitts JP, Persson P, Brown GE Jr, Parks GA (1999) Structure and bonding of Cu(II)-glutamate complexes at the gamma-Al2O3-water interface. J Colloid Interface Sci 220:133-147

Fortin D, Beveridge TJ (2000) Mechanistic routes to biomineral surface development. *In*: Biomineralization. Baeuerlein E (ed) Wiley-VCH, Weinheim, Germany, p 7-24

Fortin D, Ferris FG, Beveridge TJ (1997) Surface-mediated mineral development by bacteria. Rev Mineral 35: 161-180

Frankel RB, Bazylinski DA (2003) Biologically induced mineralization by bacteria. Rev Mineral Geochem 54:95-114

Frazer BH, Girasole M, Wiese LM, Franz T, De Stasio G (2004) Spectromicroscope for the PHotoelectron Imaging of Nanostructures with X-rays (SPHINX): performance in biology, medicine and geology. Ultramicroscopy 99:87-94

Frazer BH, Waychunas GA, Xu H, De Stasio G (2005) Quantitative mapping of the ferrous/ferric iron ratio in oxide minerals using synchrotron spectromicroscopy. Am Mineral, submitted

Fritz M, Belcher AM, Radmacher M, Walters DA, Hansma PK, Stucky GD, Morse DE (1994) Flat pearls from biofabrication of organized composites on inorganic substrates. Nature 371:49-51

Fuerst JA, Webb RI (1991) Membrane-bounded nucleoid in the eubacterium Gemmatata obscuriglobus. Proc Natl Acad Sci 88:8184-8188

Gao H, Ji B, Jäger IL, Arzt E, Fratzl P (2003) Materials become insensitive to flaws at nanoscale: lessons from nature. Proc Natl Acad Sci 100:5597-5600

Gilbert B, Banfield JF (2005) Molecular scale processes involving nanoparticulate minerals in biogeochemical systems. Rev Mineral Geochem 59:109-156

Gilbert B, Frazer BH, Belz A, Conrad PG, Nealson KH, Haskel D, Lang JC, Srajer G, De Stasio G (2003a) Multiple scattering calculations of bonding and X-ray absorption spectroscopy of manganese oxides. J Phys Chem A 107:2839-2847

Gilbert B, Frazer BH, Naab F, Fournelle J, Valley JW, De Stasio G (2003b) X-ray absorption spectroscopy of silicates for in situ sub-micrometer mineral identification. Am Mineral 88:763-769

Gilbert B, Frazer BH, Zhang H, Huang F, Banfield JF, Haskel D, Lang JC, Srajer G, De Stasio G (2002) X-ray absorption spectroscopy of the cubic and hexagonal polytypes of zinc sulfide. Phys Rev B 66(245205)

Gilbert B, Perfetti L, Fauchoux O, Redondo J, Baudat PA, Andres R, Neumann M, Steen S, Gabel D, Mercanti D, Ciotti MT, Perfetti P, Margaritondo G, De Stasio G (2000) The spectromicroscopy of boron in human glioblastomas following administration of BSH. Phys Rev E 62:1110-1118

Glasauer S, Langley S, Beveridge TJ (2001) Sorption of Fe (hydr)oxides to the surface of *shewanella putrifaciens*: cell-bound fine-grained minerals are not always formed de novo. Appl Environ Microbiol 67:5544-5550

Gotliv BA, Kessler N, Sumerel JL, Morse DE, Tuross N, Addadi L, Weiner S (2005) Asprich: a novel aspartic acid-rich protein family from the prismatic shell matrix of the bivalve Atrina rigida. Chembiochem 6: 304-314

Grush MM, Chen J, Stemmler TL, George SJ, Ralston CY, Stibrany RT, Gelasco A, Christou G, Gorum SM, Penner-Hahn JE, Cramer SP (1996) Manganese L-edge X-ray absorption spectroscopy of manganese catalase from Lactobacillus plantarum and mixed valence manganese complexes. J Am Chem Soc 118: 65-69

Han Y-J, Aizenberg J (2003) Effect of magnesium ions on oriented growth of calcite on carboxylic acid functionalized self-assembled monolayer. J Am Chem Soc 125:4032-4033

Hertz H (1887) Über einen Einfluß des ultravioletten Lichtes auf die electrische Entladung (An effect of ultraviolet light on electrical discharge). Annalen der Physik Chemie 31:983-1000

Jackson AP, Vincent JF, Turner RM (1988) The mechanical design of nacre. Proc R Soc London B 234:415-440

Juniper SK, Tebo BM (1995) Microbe-metal interactions and mineral deposition at hydrothermal vents. *In*: The Microbiology of Deep-Sea Hydrothermal Vents. Karl DM (ed) CRC Press, New York, p. 219–253

Kamat S, Su X, Ballarini R, Heuer AH (2000) Structural basis for the fracture toughness of the shell of the conch *strombus gigas*. Nature 405:1036-1040

Kaznacheyev K, Osanna A, Jacobsen C, Plashkevych O, Vahtras O, Ågren H, Carravetta V, Hitchcock AP (2002) Innershell absorption spectroscopy of amino acids. J Phys Chem A 106:3153-3168

Kemner KM, Kelly SD, Lai B, Maser J, O'loughlin EJ, Sholto-Douglas D, Cai Z, Schneegurt MA, Kulpa CF Jr, Nealson KH (2004) Elemental and redox analysis of single bacterial cells by X-ray microbeam analysis. Science 306:686-7

Kilcoyne ALD, Tyliszczak T, Steele WF, Fakra S, Hitchcock P, Franck K, Anderson E, Harteneck B, Rightor EG, Mitchell GE, Hitchcock AP, Yang L, Warwick T, Ade H (2003) Interferometer-controlled scanning transmission X-ray microscopes at the Advanced Light Source. J Synchrotron Rad 10:125-136

Labrenz M, Druschel GK, Thomsen-Ebert T, Gilbert B, Welch SA, Kemner KM, Logan GA, Summons RE, De Stasio G, Bond PL, Lai B, Kelly SD, Banfield JF (2000) Formation of sphalerite (ZnS) deposits in natural biofilms of sulfate-reducing bacteria. Science 290:1744-1747

Langley S, Beveridge TJ (1999) Effect of O-side-chain-lipopolysaccharide chemistry on metal binding. Appl Environ Microbiol 65:489-498

Lawrence JR, Swerhone GD, Leppard GG, Araki T, Zhang X, West MM, Hitchock AP (2003) Scanning transmission X-ray, laser scanning, and transmission electron microscopy mapping of the exopolymeric matrix of microbial biofilms. Appl Environ Microbiol 69:5543-5554

Lerotic M, Jacobsen C, Schafer T, Vogt S (2004) Cluster analysis of soft X-ray spectromicroscopy data. Ultramicroscopy 100:35-57

Levi-Kalisman Y, Falini G, Addadi L, Weiner S (2001) Structure of the nacreous organic matrix of a bivalve mollusk shell examined in the hydrated state using cryo-TEM. J Struct Biol 135(1):8-17

Lichtenegger HC, Schöberl T, Bartl MH, Waite H, Stucky GD (2002) High abrasion resistance with sparse mineralization: copper biomineral in worm jaws. Science 298:389-392

Lin A, Meyers MA (2005) Growth and structure in abalone shell. Mater Sci Eng A 390:27-41

Lindsay MR, Webb RI, Strous M, Jetten MS, Butler MK, Forde RJ, Fuerst JA (2001) Cell compartmentalisation in planctomycetes: novel types of structural organisation for the bacterial cell. Arch Microbiol 175:413-429

Lopez-Garcia P, Duperron S, Philippot P, Foriel J, Susini J, Moreira D (2003) Bacterial diversity in hydrothermal sediment and epsilonproteobacterial dominance in experimental microcolonizers at the Mid-Atlantic Ridge. Environon Microbiol 5:961-976

Lowenstam HA (1981) Minerals formed by organisms. Science 211(4487):1126-1131

Lowenstam HA, Weiner S (1989) On Biomineralization. Oxford University Press, Oxford

Lower SK, Hochella MF Jr, Beveridge TJ (2001a) Bacterial recognition of mineral surfaces: nanoscale interactions between Shewanella and -FeOOH. Science 292:1360-1363

Lower SK, Tadanier CJ, Hochella MF Jr (2001b) Dynamics of the mineral–microbe interface: use of biological force microscopy in biogeochemistry and geomicrobiology. Geomicrobiology J 8:63-76

Maier RM, Drees KP, Neilson JW, Henderson DA, Quade J, Betancourt JL (2004) Microbial life in the Atacama desert. Science 306:1289

Mann K, Weiss IM, Andre S, Gabius HJ, Fritz M (2000) The amino-acid sequence of the abalone (Haliotis laevigata) nacre protein perlucin. Eur J Biochem FEBS 267:5257-5264

Mann S (1988) Molecular recognition in biomineralization. Nature 332:119-124

Mann S (2001) Biomineralization: Principles and Concepts in Bioinorganic Materials Chemistry. Vol 17. Oxford University Press, Oxford

Mount AS, Wheeler AP, Paradkar RP, Snider D (2004) Hemocyte-mediated shell mineralization in the eastern oyster. Science 304(5668):297-300

Myers CR, Nealson KH (1990) Respiration-linked proton translocation coupled to anaerobic reduction of manganese(IV) and iron(III) in *Shewanella putrefaciens* MR-1. J Bacteriol 172:6232-8

Myneni SC, Tokunaga TK, Brown GE Jr (1997) Abiotic selenium redox transformations in the presence of Fe(II,III) oxides. Science 278:1106-1110

Myneni SCB (2002a) Formation of stable chlorinated hydrocarbons in weathering plant material. Science 295:1039-1041

Myneni SCB (2002b) Soft X-ray spectroscopy and spectromicroscopy studies of organic molecules in the environment. Rev Mineral Geochem 49:485-579

Myneni SCB, Brown JT, Martinez GA, Meyer-Ilse W (1999) Imaging of humic substance macromolecular structures in water and soils. Science 286:1335-1337

Nealson KH, Stahl DH (1997) Microorganisms and biogeochemical cycles: what can we learn from stratified communities? Rev Mineral 35:5-34

Newman DK, Banfield JF (2002) Geomicrobiology: how molecular-scale interactions underpin biogeochemical systems. Science 296:1071-1077

Pickering IJ, Prince RC, Salt DE, George GN (2000) Quantitative, chemically specific imaging of selenium transformation in plants. Proc Natl Acad Sci USA 97:10717-10722

Pozzolini M, Sturla L, Cerrano C, Bavestrello G, Camardella L, Parodi AM, Raheli F, Benatti U, Muller WEG, Giovine M (2004) Molecular cloning of silicatein gene from marine sponge *Petrosia ficiformis* (Porifera, Demospongiae) and development of primmorphs as a model for biosilicification studies. Marine Biotech 6:594-603

Schäffer TE, Ionescu-Zanetti C, Proksch R, Fritz M, Walters DA, Almqvist N, Zaremba CM, Belcher AM, Smith BL, Stucky GD, Morse DE, Hansma PK (1997) Does abalone nacre form by heteroepitaxial nucleation or by growth through mineral bridges? Chem Mater 9:1731-1740

Schultze-Lam S, Beveridge TJ (1994) Physicochemical characteristics of the mineral-forming S-layer from the *cyanobacterium synechococcus* strain GL24. Can J Microbiol 40:216-223

Schultze-Lam S, Thompsom JB, Beveridge TJ (1993) Metal ion immobilization by bacterial surfaces in fresh water environments. Water Poll Res J Canada 28:51-81

Shimizu K, Cha J, Stucky GD, Morse DE (1998) Silicatein alpha: Cathepsin L-like protein in sponge biosilica. Proc Natl Acad Sci USA 95:6234-6238

Shimizu K, Morse DE (2000) The biological and biomimetic synthesis of silica and other polysiloxanes. *In*: Biomineralization. Baeuerlein E (ed) Wiley-VCH, Weinheim, Germany, p 207–220

Sleytr UB (1997) Basic and applied S-layer research: an overview. FEMS Microbiol Rev 20:5-12

Smith BL, Schaffer TE, Viani M, Thompson JB, Frederick NA, Kindt J, Belcher A, Stucky GD, Morse DE, Hansma PK (1999) Molecular mechanistic origin of the toughness of natural adhesives, fibres and composites. Nature 399:761-763

Söllner C, Burghammer M, Busch-Nentwich E, Berger J, Schwarz H, Riekel C, Nicolson T (2003) Control of crystal size and lattice formation by Starmaker in Otolith biomineralization. Science 302:282-286

Stöhr J (1992) NEXAFS Spectroscopy. Springer-Verlag, Berlin

Stryer L (1995) Biochemistry, 4th edition, WH Freeman and Co, New York. See page 22.

Sturchio NC, Antonio MR, Soderholm L, Sutton SR, Brannon JC (1998) Tetravalent uranium in calcite. Science 281:971-973

Suzuki Y, Kelly SD, Kemner KM, Banfield JF (2002) Radionuclide contamination: Nanometre-size products of uranium bioreduction. Nature 419:134

Takai K, Moser DP, DeFlaun M, Onstott TC, Fredrickson JK (2001) Archaeal diversity in waters from deep South African gold mines. Appl Environ Microbiol 67:5750-5760

Tang Z, Kotov NA, Magonov S, Ozturk B (2003) Nanostructured artificial nacre. Nature Mat 2:413-418

Tebo BM, Bargar JR, Clement BG, Dick GJ, Murray KJ, Parker D, Verity R, Webb SM (2004) Biogenic manganese oxides: properties and mechanisms of formation. Ann Rev Earth Planet Sci 32:287-328

Templeton AS, Ostergren JD, Trainor TP, Foster AL, Traina SJ, Spormann A, Brown GE Jr (1999) XAFS and XSW study of the distribution of Pb(II) sorbed to biofilms on alpha-Al_2O_3 and alpha-FeOOH surfaces. J Synchrotron Radiat 6:642-644

Thompson JB, Paloczi GT, Kindt JH, Michenfelder M, Smith BL, Stucky GD, Morse DE and Hansma PK (2000) Direct observation of the transition from calcite to aragonite growth as induced by abalone shell proteins. Biophys J 79:3307-3312

Toner B, Fakra S, Villalobos M, Warwick T, Sposito G (2005) Spatially resolved characterization of biogenic manganese oxide production within a bacterial biofilm. Appl Environ Microbiol 71:1300-1310

Tonner BP, Droubay T, Denlinger J, Meyer-Ilse W, Warwick T, Rothe J, Kneedler E, Pecher K, Nealson KH, Grundl T (1999) Soft X-ray spectroscopy and imaging of interfacial chemistry in environmental specimens. Surf Interface Anal 27:247-258

Tyliszczak T, Warwick T, Kilcoyne ALD, Fakra S, Shuh DK (2004) Soft X-ray scanning transmission microscope working in an extended energy range at the Advanced Light Source. AIP Conference Proceedings, SRI. San Francisco

Urrutia M, Kemper M, Doyle R, Beveridge TJ (1992) The membrane-induced proton motive force influences the metal binding ability of *Bacillus subtilis* cell walls. Appl Environ Microbiol 58:3837-3844

Veis A (2003) Mineralization in organic matrix frameworks. Rev Mineral Geochem 54:249-289

Villalobos M, Bargar J, Sposito G (2005) Mechanisms of Pb(II) sorption on a biogenic manganese oxide. Environ Sci Technol 39(2):569-76

Weaver JC, Morse DE (2003) Molecular biology of demosponge axial filaments and their roles in biosilicification. Microscopy Res Tech 62(4):356-367

Weiner S, Dove PM (2003) An overview of biomineralization processes and the problem of the vital effect. Rev Mineral Geochem 54:1-29

Weiss IM, Kaufmann S, Mann K, Fritz M (2000) Purification and characterization of perlucin and perlustrin, two new proteins from the shell of the mollusk *haliotis laevigata*. Biochem Biophys Res Commun 267: 17-21

Zaremba CM, Belcher AM, Fritz M, Li Y, Mann S, Hansma PK, Morse DE, Speck JS, Stucky GD (1996) Critical transitions in the biofabrication of abalone shells and flat pearls. Chem Mater 8:679-690

Zawislanski PT, Benson SM, Terberg R, Borglin SE (2003) Selenium speciation, solubility, and mobility in land-disposed dredged sediments. Environ Sci Technol 37(11):2415-2420